ACS OMEGA

Open Access

http://pubs.acs.org/journal/acsodf

Article

Steric, Synergetic, Energetic Studies on the Impact of the Type of the Hybridized Polymers (Chitosan and β-Cyclodextrin) on the Adsorption Properties of Zeolite-A for Congo Red Dye

Amna M. Farhan, Gasem M. Abu-Taweel, Islam R. Sayed, Hassan Ahmed Rudayni,* Ahmed A. Allam, Wail Al Zoubi,* and Mostafa R. Abukhadra*

Cite This: *ACS Omega* 2024, 9, 21204−21220

Read Online

ACCESS | Metrics & More | Article Recommendations | Supporting Information

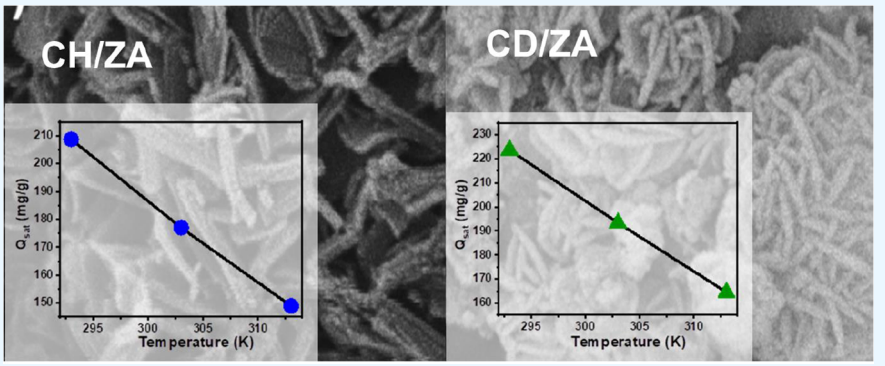

ABSTRACT: Zeolite-A was synthesized successfully from kaolinite and hybridized with two species of biopolymers (chitosan (CH/Z) and β-cyclodextrin (CD/Z)). The obtained hybridized forms were assessed as potential adsorbents of Congo red synthetic dye (CR) with enhanced affinities and elimination capacities. The synthesized CD/Z and CH/Z hybrids demonstrated uptake capacities of 223.6 and 208.7 mg/g, which are significantly higher than single-phase zeolite-A (140.3 mg/g). The integrated polymers change the surface area, surface reactivity, and number of free active receptors that are already present. The classic isotherm investigations validate Langmuir equilibrium behavior for ZA and Freundlich properties for CD/Z and CH/Z. The steric parameters validate a strong increase in the existing active receptors after the incorporation of CD (CD/Z) to be 98.1 mg/g as compared to 83 mg/g for CH/Z and 60.6 mg/g for ZA, which illustrate the detected uptake behaviors. Moreover, the CR dye was adsorbed as several molecules per single site, reflecting the vertical uptake of these molecules by multimolecular mechanisms. The energetic assessment, considering both Gaussian energies and adsorption energies (<40 kJ/mol), validates the dominant impact of the physical mechanism during the sequestration of CR (dipole binding interactions (2−29 kJ/mol) and hydrogen bonds (<30 kJ/mol)), in addition to the considerable effect of ion exchange processes. Based on the thermodynamic parameters, the CR molecules were adsorbed by exothermic and spontaneous reactions.

INTRODUCTION

The main risk confronting the modern world is the contamination of drinking water, along with the security of its citizens.[1,2] The World Health Organization (WHO) released an urgent warning that, as early as 2025, half of the globe's inhabitants would face a significant shortage of water.[2,3] The rapid expansion of industry in the last century has led to serious environmental problems, including water pollution and its detrimental impact on both humans and marine ecosystems.[1,4] Industrial operations emit a range of water contaminants, such as microorganisms, insecticides, toxic metals, medicinal residues, fertilizer, and dyes.[5] Artificial dyes are a diverse group of aromatic chemicals that are widely used as essential coloring materials in many sectors, such as plastic, paper, leather, and textiles.[6,7] Consequently, an approximate quantity of more than 700,000 tons of the produced dyes was discharged throughout the neighboring regions and aquatic habitats each year.[8]

Most chemically produced dyes are poisonous and bioresistant compounds, which can exert detrimental effects on the natural environment and human well-being.[3,8] Congo red, also known as amino-1-aminonaphthalene sulfonic, is a widely used type of acidic azo dye. It is frequently

Received: February 4, 2024
Revised: April 5, 2024
Accepted: April 17, 2024
Published: April 30, 2024

implemented in printing, leather production, the manufacture of paper, the polymer industry, and textile dyeing.[9,10] Nevertheless, the migration of CR toward crucial drinking water resources as solution-soluble organic contaminants poses significant toxicity and severe environmental consequences.[10,11] The dissolved CR results in a decrease in the oxygen content within the water supplies and disrupts the normal functioning of the photosynthesis mechanism, resulting in negative effects on the marine ecosystem.[4] The accidental release of CR dye into lakes and rivers has a significant negative impact on the well-being of people and aquatic life owing to its very limited biodegradability and the mutagenic and carcinogenic properties of its converted benzidine form. This might result in symptoms that include diarrhea, nausea, allergies, vomiting, and digestive irritation in humans.[12−14] The azobenzene constituent of CR has been recognized to have a possible carcinogenicity factor of 1.08×10^{-1} (mg/kg/day) if consumed orally.[15]

Various methods have already been established to eliminate the dye pollutants, based on the earlier mentioned health and environmental issues. These methods include ozonation,[16] photocatalytic degradation,[17] coprecipitation,[18] flocculation/coagulation,[19] adsorption,[20] and ion exchange[21] technologies. The cost-effective value of the adsorbing approach, along with its ability to efficiently remove dyes, including Congo red, renders it a highly endorsed elimination technique. This approach offers advantages such as excellent eliminating capacity, wide applicability, simplistic recovery and recycling capacity, and affordable manufacturing practices.[22,23] Therefore, various types of mono and hybrid structures have been explored to develop effective adsorption agents against dyes.[2,3,24] Nevertheless, the key considerations in selecting the most appropriate adsorbents are their manufacturing expenses, natural abundance, rapid kinetic rates, retention effectiveness, adsorption specificity, and reuse and recovery values.[25]

Subsequently, multifunctional and hybrid frameworks comprising different organic/inorganic reacting functional groups derived from naturally occurring precursors have been investigated as enhanced affordable adsorbents for organic compound purification.[26,27] The latest studies highlight the promise of using synthetically produced zeolite/biopolymers as cost-effective and multifunctional adsorption agents. These materials possess outstanding adsorption performances, regeneration possibilities, ion exchange efficiency, biodegradable characteristics, and ecological advantages.[28,29] The prepared variations of zeolite were widely highlighted for their exceptional physical, chemical, and textural qualities. These forms can be successfully blended with different components to establish a hybrid framework that exhibits enhanced properties.[28,30] Synthetically produced zeolite-A possesses significant structural versatility, surface area, chemical stability, nontoxicity, adsorption efficiency, and biological compatibility.[31,32] An important limitation during the qualification and application of zeolite-A is its strong hydrophilicity, which negatively impacts its ability to interact with organic chemicals existing within water.[33] To mitigate this, several approaches were employed to modify the exterior of zeolite through different types of polymers, organic compounds, and organic surfactants. This can enhance the affinity of zeolite for organic compounds and increase its reactivity. Additionally, this could enhance the arrangement of pore sizes within the structure and, in turn, its measured surface area.[34,35]

Chitosan is a well-established biopolymer that is frequently employed in many applications.[36,37] It is derived by facile methods using chitin, which is prevalent in several biological resources and has notable commercial advantages.[38] It possesses notable biological activity, safety, and biodegradability, along with excellent adsorption qualities.[36] β-cyclodextrin (β-CD) polymer is also a frequently utilized and important biopolymer that was thoroughly examined as a vital constituent for multiple blends with distinct inorganic ingredients for various uses.[39,40] This was assigned for its great availability, notable chemical resistance, nontoxic nature, and valuable adsorption properties.[41,42] β-CD comprises a cyclic glucopyranose composed of up to seven glucose units that are connected to one another by various types of (1→ 4) glycosidic linkages.[34,40] The β-CD's basic units have a highly polar external surface, whereas the inner structure exhibits hydrophobic properties.[36] This significantly promotes its integration into hybrids containing inorganic components and enhances the capacity of synthesized structures to accommodate soluble organic compounds.[41,43]

The hybridization of chemically produced zeolite-A using chitosan and β-CD chains was speculated to yield a novel hybrid structure. These structures were intended to have improved adsorption properties and a greater number of active sites corresponding to the inserted chemical groups. The objective of this enhancement was to enable better elimination of CR dye in contrast to employing synthetic zeolite alone. The current investigation focused on developing and evaluating CH/Z and CD/Z hybrids as more effective adsorbents for acidic Congo red dye in water-based solutions. This entailed a thorough examination of the manner in which the incorporation of polymers affects the adsorption behaviors, quantity of existing active sites, occupation performances, and textural characteristics of ZA, energetic qualities, and regulating mechanisms. This analysis investigated the frequently examined kinetic and isotherm mathematical models, together with advanced equilibrium investigations utilizing statistical physics theory alongside the corresponding steric and energetic factors.

2. RESULTS AND DISCUSSION

2.1. Characterization of the Used Adsorbents. The synthesized zeolite integrated into the two blends has the typical X-ray diffraction (XRD) pattern of ZA (Figure 1). The distinct peaks have been observed around specific angles of 7.20, 10.32, 12.60, 16.2, 21.83, 26.20, 27.20°, 30.90, 33.39, and 34.30°, as reported by ref 45 (Figure 1A). In terms of the detected pattern of incorporated chitosan, it resembles the semicrystalline features of marketable chitosan, comprising two wide peaks approximately around 9.91 and 20.22°[38] (Figure 1B). The observed pattern of the fabricated CH/Z indicates a remarkable interaction among the two constituents of the blend. Multiple distinct peaks of zeolite exhibited significant reduction, along with a noticeable shift in their locations (15.48, 21.65, 25.52°, 27.11, and 30.6°) (Figure 1C). The marked pattern corresponding to β-CD exhibits the distinctive peaks of commonly utilized crystallized β-CD (6.8, 10.83, 12.57, 12.8, 13.0, 18.9, 21.90, 23, 27.34, and 34.90°) (Figure 1D). For the blended zeolite-A together with β-CD, the evaluated pattern confirms the presence of complex peaks corresponding to both components although there are obvious shifts in the locations (Figure 1E). The remaining peaks of

https://doi.org/10.1021/acsomega.4c01134
ACS Omega 2024, 9, 21204−21220

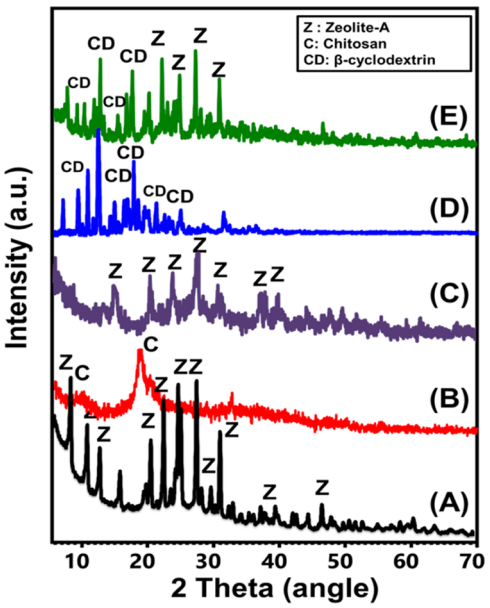

Figure 1. XRD patterns of zeolite-A (A), chitosan (B), CH/Z composite (C), β-cyclodextrin (D), and CD/Z composite (E).

zeolite-A have been identified at certain angles: 7.25, 10.26, 12.50, 21.75, 26.70, 27.2, 30.0, 30.96, and 32.66°. Additionally, other persistent peaks of CD have been observed at angles of 8.94, 10.26, 18.83, and 26.19° (Figure 1E).

The synthesized zeolite used in the study displays the distinctive cubic shape common to zeolite-A (Figure 2A). The acquired scanning electron microscopy (SEM) photos confirm significant alterations in the exterior geometry of the CH/Z as compared to the ZA (Figure 2B,C). The ZA granules exhibited a significant coating of the chitosan matrix (Figure 2B,C). The high-magnified views reveal the presence of interlocked rod-like particulates, comprising another nanoporous network (Figure 2B,C). The high-resolution transmission electron microscopy (HRTEM) photos of CH/Z exhibit congruence with the distinct geometries observed in the SEM photos (Figure 2D,E). The cubic granules of ZA have been detected as entrapment fractions inside the framework of the chitosan (Figure 2D). Furthermore, the intersecting of the chitosan rod-like particulates is clearly discernible, as is the development of a porous matrix (Figure 2E). Similar changes in morphology have been detected for CD/Z; the resulting particulates exhibit significant aggregation characteristics (Figure 2F,G). The ZA granules inside the aggregated CD/Z particulates display considerable random realignment, leading to notable rough surface characteristics (Figure 2F,G). The marked granules noticed in the SEM magnified photos had bent platelet shapes at the nanoscale, and their interlocking resulted in flower-like patterns with noticeable pores in between (Figure 2G). The HRTEM photos demonstrate that the ZA granules have a random distribution throughout the blocky framework of β-CD (Figure 2H). Furthermore, the flower-like structures are clearly visible in the inspected photos (Figure 2I).

The blending processes also significantly affected the surface area of the final-yield composites. The starting surface area of ZA, measured at 423 m^2/g, was significantly increased to 446.7 and 457.2 m^2/g after undergoing hybridization with CH (CH/Z) and β-CD (CD/Z), respectively (Table 1). The increased surface area facilitates a highly interactive contact between the CH/Z and CD/Z and the soluble dye molecules. The results also revealed a slight rise in the overall pore volume of ZA (0.382 cm^3/g), with values of 0.412 cm^3/g for CH/Z and 0.433 cm^3/g for CD/Z. Additionally, there was a rise in the mean pore dimension to 23.6 nm for CH/Z and 20.4 nm for

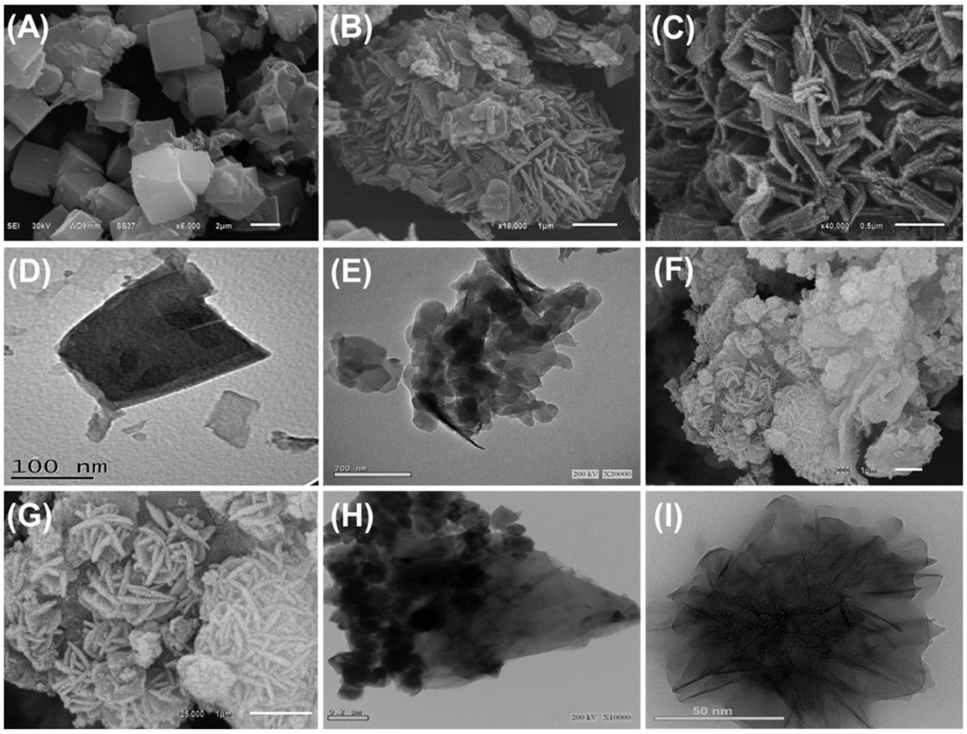

Figure 2. SEM image of zeolite-A (A), SEM images of the prepared CH/Z composite (B, C), HRTEM images of the prepared CH/Z composite (D, E), SEM images of the prepared CD/Z composite (F, G), and HRTEM images of the prepared CH/Z composite (H, I).

https://doi.org/10.1021/acsomega.4c01134
ACS Omega 2024, 9, 21204−21220

Table 1. Textural Properties of ZA, CH/Z, and CD/Z

sample	specific surface area (m^2/g)	total pore volume (cm^3/g)	average pore size (nm)
ZA	423	0.382	11.6
CH/Z	446.7	0.412	23.6
CD/Z	457.2	0.433	20.4

CD/Z instead of 11.6 nm for ZA (Table 1). The observed textural characteristics mostly resulted from significant changes in the geometrical characteristics of ZA particulates following the incorporation of the polymer compounds, as well as the presence of further pores corresponding to the framework of polymers along with the interlocking of their particles.

The Fourier transform infrared (FT-IR) spectrum (Figure 3) effectively revealed the key chemical structures of ZA. This

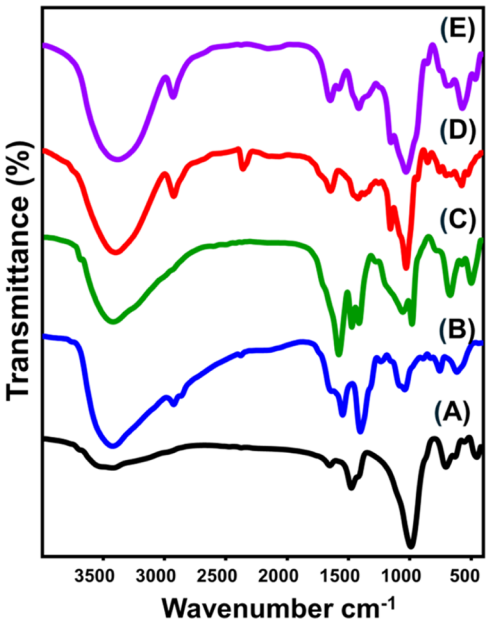

Figure 3. FT-IR spectra of zeolite-A (A), chitosan (B), CH/Z composite (C), β-cyclodextrin (D), and CD/Z composite (E).

comprises Si−O (452 and 705 cm^{-1}), Si−O−Al (555 and 630 cm^{-1}), Si−OH (3612 cm^{-1}), Si−O−Si (990 cm^{-1}), Al−OH (3422 cm^{-1}), zeolitic water (1475 cm^{-1}), and OH stretching (1650 cm^{-1}) (Figure 3A).[46,47] The key chemical groups of CH have also been identified clearly, including C−N (1402 cm^{-1}), N−H (1547 cm^{-1}), C−H (2925 and 1336 cm^{-1}), OH (3423 cm^{-1}), C−O (1040 cm^{-1}), and C═O (1637 cm^{-1})[36,38] (Figure 3B). The CH/Z spectrum reveals the effective combining and synergy between CH and the ZA chemical structures (Figure 3C). The key functional groups of both CH (C−O (1059 cm^{-1}), N−H (1582 cm^{-1}), and C−H (1416 cm^{-1})) and ZA (Si−O−Si (938 cm^{-1}), zeolitic water (1475 cm^{-1}), Si−O (298 cm^{-1}), and Si−O−Al (671 cm^{-1})) were reported during the evaluation of the spectrum of their blend. These groups were seen at varying places in the spectrum.

The β-CD spectrum exhibited well-defined peaks at specific positions corresponding to O−H (3376 cm^{-1}), $-CH/CH_2$ bonds (2926 cm^{-1}), C−C or H−O−H deformation (1666 cm^{-1}), C−OH (1482 cm^{-1}), C═O or OH (1636 cm^{-1}), glycosidic C−O−C (1158 cm^{-1}), C−O (1000 cm^{-1}), and C−O−C (1200 cm^{-1}) (Figure 3D).[36,39] The recognized spectrum of CD/Z clearly indicates the successful development of hybrids comprising both β-CD and ZA particles (Figure 3E). The fundamental chemical groups of β-CD have been recognized as C−OH (2930 cm^{-1}), glycosidic C−O−C (1152 cm^{-1}), and C−OH (1578 cm^{-1}). Additionally, the fundamental chemical groups of ZA have been recognized as Si−O−Si (1030 cm^{-1}), Al−OH (3388 cm^{-1}), Si−O−Al (695 cm^{-1}), zeolitic water (1415 cm^{-1}), and Si−O (858 cm^{-1}) (Figure 3E).

2.2. Adsorption Studies. *2.2.1. Effect of pH.* The pH variable plays an essential function throughout the adsorption process as it influences both the exterior charges of the adsorbent and the ionizing activity of soluble contaminants within the water-based solutions. The study examined the adsorption properties of ZA, CH/Z, and CD/Z for the elimination of CR. The investigation included a pH range of 3 to 8, while keeping other factors consistent at the following selected levels: an initial volume of 100 mL, a level of concentration equal to 100 mg/L, a duration of 120 min, a mass of 0.4 g/L, and testing at 20 °C. According to the results obtained by measuring the quantities of CR adsorbed employing ZA, CH/Z, and CD/Z, it is evident that there was a significant decrease in the absorption of CR whenever the pH level of the examined contaminated solutions shifted beyond pH 3 (Figure 4). The uptake characteristics decreased

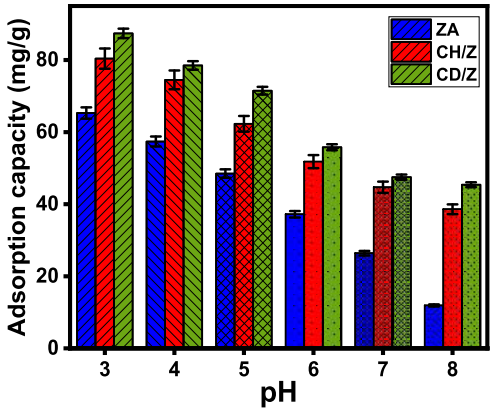

Figure 4. Impact of the solutions pH on the adsorption efficiencies of CR dye by ZA, CH/Z, and CD/Z (volume: 100 mL; concentration: 100 mg/L; duration: 120 min; mass: 0.4 g/L; temperature: 20 °C).

from 65.3 mg/g (ZA), 80.4 mg/g (CH/Z), and 87.3 mg/g (CD/Z) at pH 3 down to 11.9 mg/g (ZA), 38.6 mg/g (CH/Z), and 45.4 mg/g (CD/Z) at pH 8 (Figure 4). The zero points of charge's pH ($pH_{(ZPC)}$) values are 5.1 for ZA, 4.5 for CH/Z, and 3.8 for CD/Z, which are consistent with prior findings about the dominance of negative charges beyond these values.

Consequently, the assessed structures could be considered suitable to be implemented as successful adsorbents for practical treatment procedures for CR, according to the pH range of industrial effluent specified through the US EPA (pH 6 to 9) alongside the observed performance of the assessed structures at different pH levels.[48] The ionizing behavior of CR dye alongside the prevailing surface charges across the frameworks of ZA, CH/Z, and CD/Z may be used to illustrate the reported variations in the uptake behaviors. Regarding the ionizing properties of CR, the acidic CR molecules with their negative charges exhibit strong electrostatic attraction toward

https://doi.org/10.1021/acsomega.4c01134
ACS Omega 2024, 9, 21204−21220

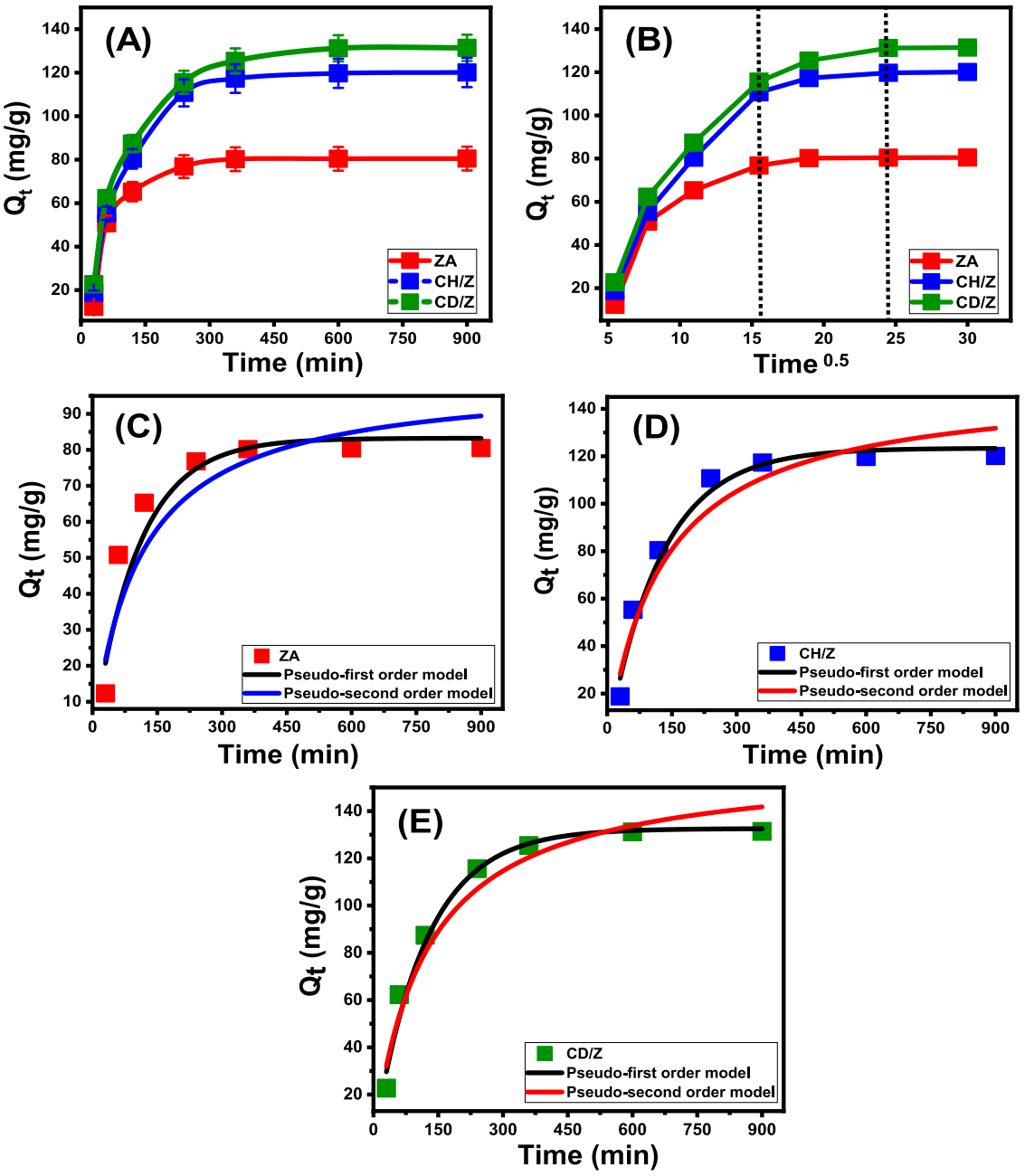

Figure 5. Experimental impact of uptake duration on the adsorption of CR dye by ZA, CH/Z, and CD/Z (CR level (100 mg/L), pH (3), volume (100 mL), temperature (20 °C), and mass (0.4 g/L)) (A). The intraparticle diffusion curves of the CR adsorption (B) and fitting of the CR adsorption results with the classic kinetic model (ZA (C), CH/Z (D), and CD/Z (E)).

the positively charged functional groups of ZA, CH/Z, and CD/Z at low pH conditions (acidic environment).[11,48−50]

2.2.2. Kinetic Studies. 2.2.2.1. Effect of Contact Time. An experiment has been conducted to investigate how the time frame of CR removal affects the characteristics of ZA, CH/Z, and CD/Z. The examination was completed in a time frame that spanned from 30 to 900 min. The specified levels of time were evaluated after maintaining the other essential factors, including CR level (100 mg/L), pH (3), volume (100 mL), temperature (20 °C), and mass (0.4 g/L). The effectiveness of ZA, CH/Z, and CD/Z during the uptake process of CR demonstrates significant improvement in the actual removal rates along with the established quantity of CR adsorbed. Moreover, it is essential to realize that the time frame of the examinations has a significant controlling impact on the confirmed increments in the uptake behaviors described before (Figure 5A). The CR uptake patterns are significantly improved by utilizing ZA and CH/Z for 360 and 600 min for CD/Z. Following the prescribed periods of interaction, there had been no noticeable changes or improvements either in the rates of CR elimination or in the amounts of CR retained. Based on prior investigation, it can be concluded that ZA, CH/Z, and CD/Z adsorbents established their levels of stability following the previously mentioned durations, which correspond to the intervals of the equilibrium stages throughout the CR retention (Figure 5A). The equilibrium retention capacities of CR on ZA, CH/Z, and CD/Z have been established to be 80.5, 120.1, and 131.4 mg/g, respectively

https://doi.org/10.1021/acsomega.4c01134
ACS Omega 2024, 9, 21204−21220

Table 2. Mathematical Parameters of the Addressed Kinetic Models

models	parameters	ZA	CH/Z	CD/Z
pseudo-first-order	K_1 (1/min)	0.0095	0.008	0.008
	$Qe_{(Cal)}$ (mg/g)	83.2	123.4	132.59
	R^2	0.926	0.97	0.98
	χ^2	2.25	0.97	0.74
pseudo-second-order	k_2 (g/(mg·min))	9.14×10^{-5}	5.09×10^{-5}	5.15×10^{-5}
	$Qe_{(Cal)}$ (mg/g)	100.27	150.84	160.77
	R^2	0.89	0.95	0.96
	χ^2	3.26	1.95	1.48

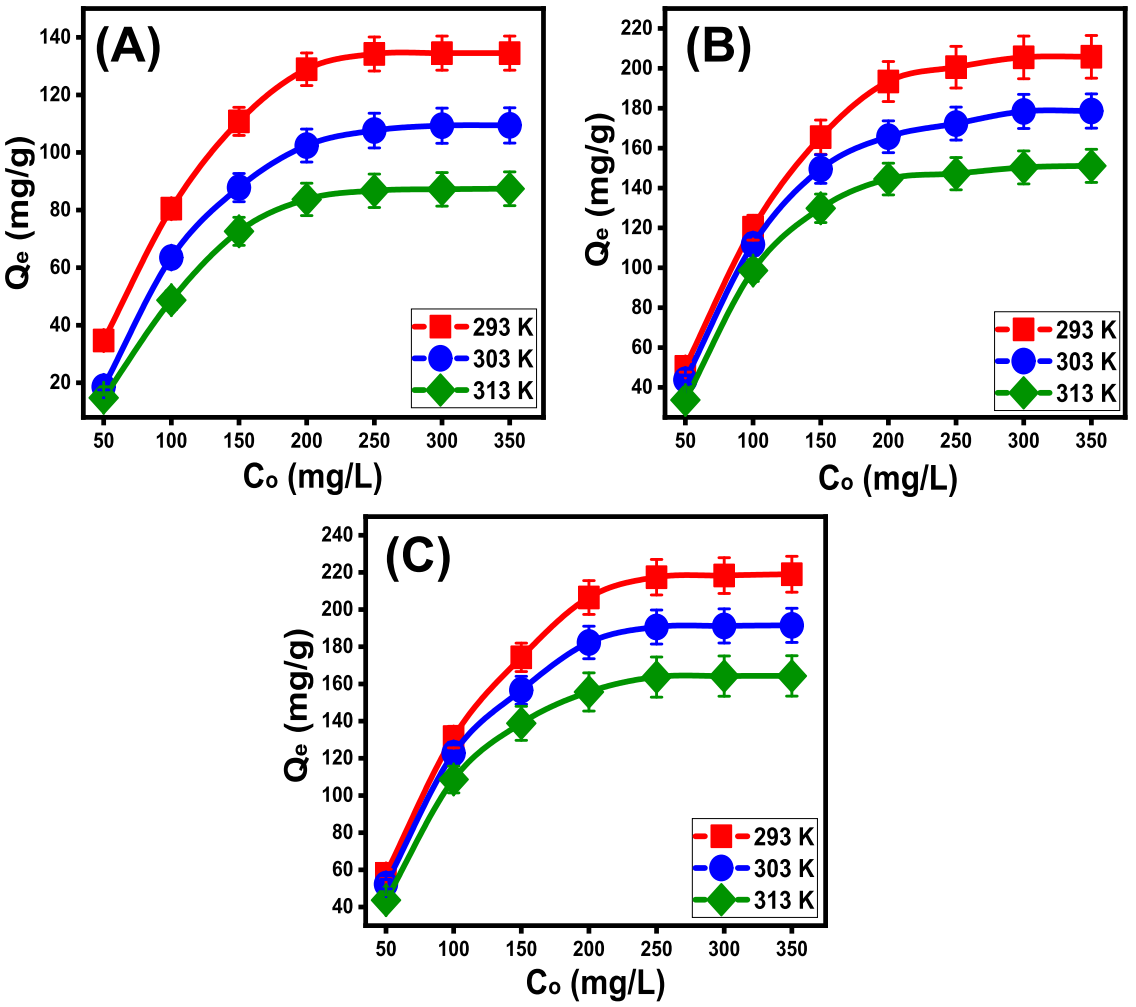

Figure 6. Experimental impact of starting CR concentration on the uptake capacities of ZA (A), CH/Z (B), and CD/Z (C).

(Figure 5A). The initial stages of the testing associated with the presence of an extensive number of reactive and free binding sites or receptors throughout the frameworks of ZA, CH/Z, and CD/Z led to strong improvements and increases in the rates of CR removal and the amounts of CR adsorbed.[42] Extended durations of testing lead to a significant decrease in the quantity of unoccupied receptors. This is mostly caused by the prolonged adsorption of CR, which subsequently results in the occupation of these receptors and a reduction in the availability of free or empty receptors. Consequently, the rates of CR adsorption exhibited a substantial drop after a particular time frame. Also, the bindings of CR by ZA, CH/Z, and CD/Z displayed stable properties or exhibited minimal enhancement. Whenever all receptors or possible interaction sites are occupied by CR, the equilibrium states of ZA, CH/Z, and CD/Z have been established, and more dye molecules can be achieved.[51]

2.2.2.2. Intraparticle Diffusion Behavior. The evaluation of CR uptake behaviors utilizing ZA, CH/Z, and CD/Z could theoretically be analyzed by assessing their intraparticle diffusion trends. The displayed curves exhibit three distinct segments characterized by different slopes (Figure 5B). The continuing investigation indicates that the observed curves are not consistent with their initial points, indicating the presence of various additional adsorption mechanisms in addition to the diffusion paths of CR.[52,53] The operated mechanisms might generally encompass three crucial phases: (1) the interaction between CR and the unoccupied receptors distributed

https://doi.org/10.1021/acsomega.4c01134
ACS Omega 2024, 9, 21204−21220

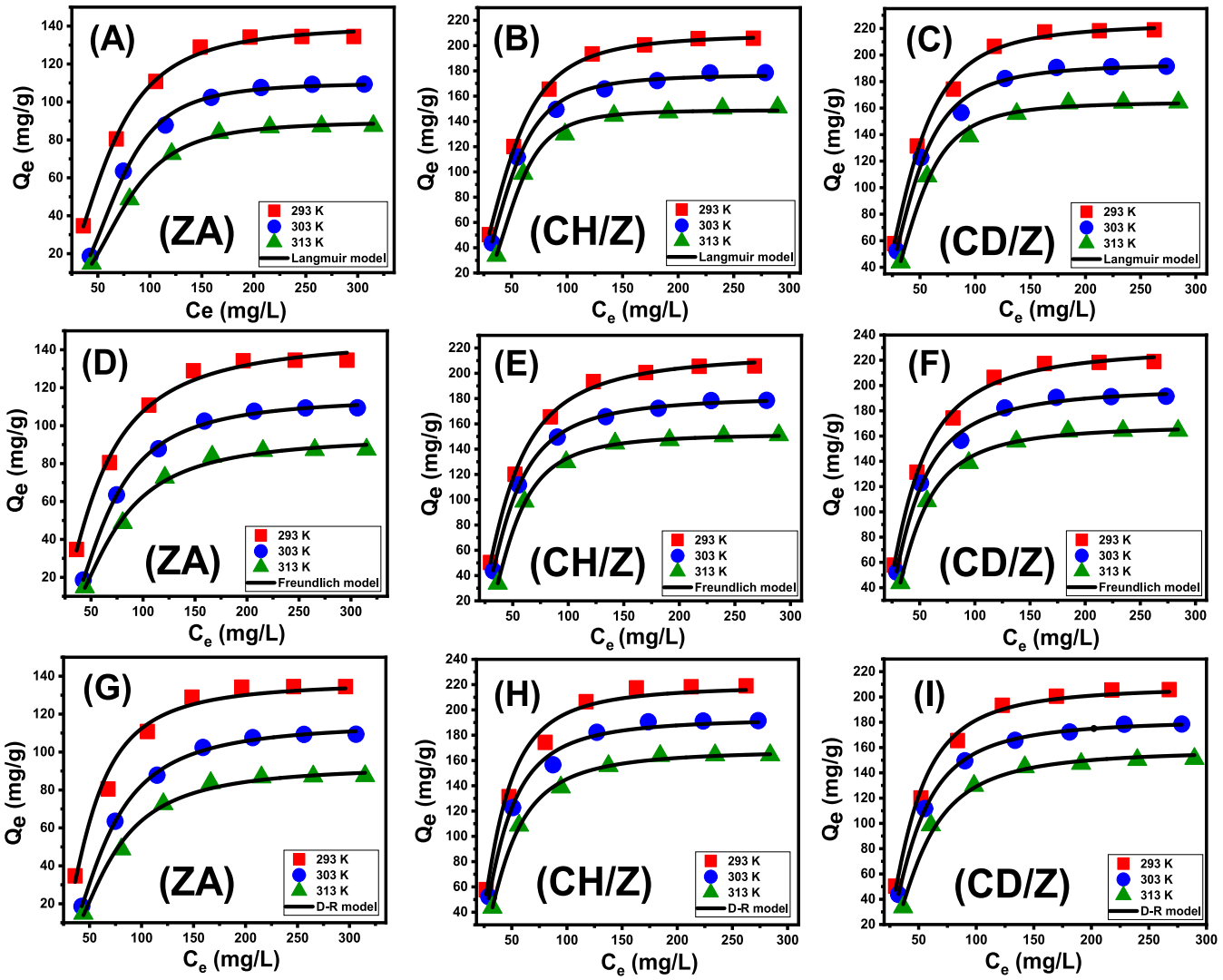

Figure 7. Fitting of the CR adsorption results with the classic Langmuir isotherm model (ZA (A), CH/Z (B), and CD/Z (C)), classic Freundlich model (ZA (D), CH/Z (E), and CD/Z (F)), and classic D−R model (ZA (G), CH/Z (H), and CD/Z (I)).

throughout the external interfaces of ZA, CH/Z, and CD/Z (boundary); (2) the layered uptake of CR and the diffusion behaviors of the CR; (3) the influence of saturated state and stabilization situations.[54] The initial outcomes of these investigations indicate that the main mechanisms responsible for anchoring CR to the exterior surfaces of ZA, CH/Z, and CD/Z (external adsorption) were the most influential paths recognized during the entire investigation (Figure 5B). The effectiveness of CR adsorbing throughout this phase is dependent upon the total amounts of receptors located across the interaction surfaces of ZA, CH/Z, and CD/Z.[55] Extending the duration enhanced the identification of the subsequently developed mechanistic phase and emphasized the efficacy of further layered adsorption processes after the full consumption of all of the exterior receptors (Figure 5B).[25,55] Moreover, these supplemental mechanisms include the implications of CR diffusion activities. As ZA, CH/Z, and CD/Z eventually attained equilibrium with respect to CR binding, the final mechanistic phases exhibited a substantial influence. This indicates that the entire quantity of CR molecules that have been effectively adsorbed has occupied all of the available binding sites.[36,56] The elimination of CR throughout this phase involves molecular interactions and interionic attraction mechanistic paths.[36]

2.2.2.3. Kinetic Modeling. The traditional kinetic theories of pseudo-first-order (P.F.) as well as pseudo-second-order (P.S.) mathematical models were used to examine the kinetic aspects of CR reduction mechanisms using ZA, CH/Z, and CD/Z. The fitness levels of the CR sequestration processes and kinetic concepts with respect to the two theories have been evaluated by employing nonlinear fitting variables according to the respective equations and estimated through the use of the coefficient of determination (R^2) in addition to the Chi-squared (χ^2) (Table 2; Figure 5C,D,E). The R^2 values accomplished, in conjunction with the χ^2 data, reveal that the kinetic characteristics as well as the concepts of the P.F. model provide a more precise match for the adsorption behaviors of CR utilizing ZA, CH/Z, and CD/Z, in comparison to the evaluated P.S. hypothesis. The experimental findings for ZA (80.5 mg/g), CH/Z (120.1 mg/g), and CD/Z (131.4 mg/g) during equilibrium levels closely corresponded to the values derived from theoretical computations utilizing the P.F. model (ZA (83.2 mg/g), CH/Z (123.4 mg/g), and CD/Z (132.6 mg/g)) (Table 2). The observed agreement further confirms the previously reported results emphasized in

https://doi.org/10.1021/acsomega.4c01134
ACS Omega 2024, 9, 21204−21220

the kinetic assessment about the better fitness of the P.F. model (Table 2). The P.F. hypothesis posits that the sequestration of CR onto ZA, CH/Z, and CD/Z is primarily influenced by physical processes, including van der Waals forces or electrostatic attraction.[57,58] The analyzed uptake properties also show significant conformity with the P.S. hypothesis; however, the P.F. modeling offers greater favorable agreement. Previous studies have demonstrated that frequently encountered chemical implications, including hydrogen bonding, complexing, and hydrophobic interactions, have the potential to either improve or have a minimal impact on the elimination of CR via ZA, CH/Z, and CD/Z.[53,57] Successive CR adsorbed layers can be developed via physical methods utilizing the previously formed chemically binding CR layer as a foundation.[59]

2.2.3. Equilibrium Studies. 2.2.3.1. Effect of Cd (II) Concentrations. The investigation aimed to define the upper limits of ZA, CH/Z, and CD/Z's uptake capacities and establish their equilibration settings within the evaluated range of 50 to 350 mg/L by examining the impact of initial CR contents. The other parameters affecting elimination were maintained steady at specified values, including an entire volume equal to 100 mL, a period equal to 24 h, a mass of 0.4 g/L, and a temperature range from 293 to 313 K. The notable enhancement in the quantity of CR adsorbed across ZA, CH/Z, and CD/Z might be attributable to the elevated concentrations of CR (Figure 6A−C). The elevation in the concentration of CR inside a specific volume resulted in a substantial improvement in the dispersing, driving forces, and diffusion behaviors of these soluble compounds. This enabled interactions with a greater quantity of the functioning receptors that existed in ZA, CH/Z, and CD/Z. Therefore, the CR retention activities performed by ZA, CH/Z, and CD/Z displayed significant increases in effectiveness in terms of the evaluated CR contents.[60] A strong correlation has been established between the starting concentrations and the quantifiable quantity of CR removal; however, this interaction can only be detected up to certain limitations. Furthermore, expanding the starting level of CR appears to have little impact on the uptake of CR onto ZA, CH/Z, and CD/Z. The distinction between the states of equilibration facilitates determining the specific maximal retention capacity of CR. The CR retention capacities of ZA are 134.5 mg/g at 293 K, 109.4 mg/g at 303 K, and 87.5 mg/g at 313 K (Figure 6A). The equilibration capacities of CR for CH/Z are 205.8 mg/g at 293 K, 178.6 mg/g at 303 K, and 151 mg/g at 313 K (Figure 6B). The CR sequestration capacities for CD/Z at different temperatures are as follows: 219 mg/g at 293 K, 191.5 mg/g at 303 K, and 164.3 mg/g at 313 K (Figure 6C). The better uptake characteristics exhibited by CH/Z and CD/Z as opposed to ZA might be attributed to three factors: (1) the increased surface area; (2) the substantial enhancement in the organophilic properties of CH/Z and CD/Z in comparison to the hydrophilic zeolite; (3) a substantial boost in the overall number of binding sites caused by the incorporation of CH and CD. The observed decrease in CR uptake when utilizing ZA, CH/Z, and CD/Z at various temperatures suggests that the analyzed processes exhibit exothermic properties.

2.2.3.2. Giles's Classification. The isotherm trends of CR adsorption, using ZA, CH/Z, and CD/Z, were classified according to the specifications provided in Giles' classifications. The study indicated that the assessed curves exhibited an L-type equilibrium class (Figure 6A−C). The isotherm properties of the L-type equilibrium demonstrate the notable effects resulting from intermolecular attractive interactions that occur during the removal activities of CR using ZA, CH/Z, and CD/Z (Figure 6A−C). The aforementioned behaviors are enhanced by the intense interactions of CR, which occur across the very reactive interfaces of ZA, CH/Z, and CD/Z.[61] Based on the specifications of the L-type class, it was expected that ZA, CH/Z, and CD/Z particulates had entire layers of sequestrated CR formed on their exteriors.[62] Additionally, the detected isothermal state reveals that the ZA, CH/Z, and CD/Z particles have an extensive variety of significant and efficient sites for adsorption. Also, the binding sites demonstrate significant affinities toward the CR molecules, especially if the initial CR levels are low.

2.2.3.3. Classic Isotherm Models. The Langmuir (Figure 7A−C), Freundlich (Figure 7D−F), and Dubinin−Radushkevich (D−R) (Figure 7G−I) equilibrium principles have been employed to assess the isotherm specifications of CR sequestration behaviors using ZA, CH/Z, and CD/Z. These theories and their illustrated nonlinear equations are shown in Table 3. The degree of agreement between the reported equilibrium hypotheses of the aforementioned models and the experimentally inspected CR sequestrated behaviors was assessed by employing nonlinear fitting methods that use the corresponding equations for such models. The evaluation included analyzing the coefficient of determination (R^2) paired with the Chi-squared (χ^2) results. The findings obtained from the analysis of R^2 and χ^2 indicate that the ZA particles exhibit CR retention characteristics that are better compatible with Langmuir's concepts than the Freundlich hypothesis. This isothermal behavior reflects the uniform or homogeneous binding tendency of CR across the unoccupied and reactive receptors of ZA particles in a single or monolayer formation.[57,58] The uptake characteristics of CR through CH/Z and CD/Z might possibly be elucidated by employing the concepts of equilibrium, as outlined through the Freundlich formula, and implementing the supplied fitting variables. This indicates that the binding of CR across the CH/Z and CD/Z hybrids is accomplished with a heterogeneous approach, with the adsorbed molecules being dispersed across the interfaces of the blends in multilayered forms. Moreover, studies have demonstrated that ZA, CH/Z, and CD/Z particulates have CR-retaining behaviors with RL (separation factor) values below 1, confirming the favorable characteristics of these processes.[55,56] The greatest adsorption qualities (Q_{max}) of CR for ZA at different temperatures, as determined by mathematical calculations, are 140.3 mg/g at 293 K, 110 mg/g at 303 K, and 89.6 mg/g at 313 K (Table 3). The computed values of CH/ZA are 208.7 mg/g at 293 K, 177 mg/g at 303 K, and 148.9 mg/g at 313 K (Table 3). The results achieved by utilizing the CD/Z method are as follows: 223.6 mg/g at 293 K, 193.3 mg/g at 303 K, and 164.5 mg/g at 313 K (Table 3).

The equilibrium aspects of the D−R theories offer a comprehensive understanding of the energetic variations demonstrated by ZA, CH/Z, and CD/Z particles throughout CR sequestration activities, irrespective of the structure's degree of homogeneity or heterogeneity.[63] Examining the D−R model findings is essential for ascertaining the Gaussian energy (E) and comprehending the underlying mechanisms (chemical or physical) responsible for retaining CR. Prior studies have verified that adsorption processes display E levels less than 8 kJ/mol, between 8 and 16 kJ/mol, and higher than

https://doi.org/10.1021/acsomega.4c01134
ACS Omega 2024, 9, 21204−21220

Table 3. Mathematical Parameters of the Addressed Classic Isotherm Models

		ZA			CH/Z			CD/Z		
models	parameters	293 K	303 K	313 K	293 K	303 K	313 K	293 K	303 K	313 K
Langmuir	Q_{max} (mg/g)	140.36	110.04	89.6	208.7	177.03	148.9	223.6	193.3	164.5
	b (L/mg)	8.06×10^{-5}	1.4×10^{-6}	1.9×10^{-6}	6.26×10^{-5}	1.42×10^{-5}	8.79×10^{-7}	1.91×10^{-4}	8.92×10^{-5}	2.16×10^{-5}
	R^2	0.99	0.994	0.991	0.999	0.998	0.997	0.996	0.993	0.995
	χ^2	0.048	0.068	0.013	0.04	0.09	0.1	0.15	0.2	0.12
Freundlich	$1/n$	0.56	0.44	0.47	0.51	0.44	0.37	0.54	0.5	0.45
	k_F [(mg/g)(l/mg)$^{1/n}$]	146.4	114.6	94.04	215.6	181.4	151.8	230.5	198.1	168.1
	R^2	0.987	0.991	0.974	0.99	0.997	0.995	0.997	0.996	0.998
	χ^2	0.461	0.124	0.257	0.04	0.01	0.02	0.11	0.11	0.04
D−R	β (mol^2/KJ^2)	0.00794	0.0164	0.0213	0.0056	0.0063	0.0083	0.0043	0.0047	0.006
	Q_{D-R} (mg/g)	136.58	115.04	92.46	207.9	181.6	157.7	219.05	193.28	167.99
	R^2	0.988	0.999	0.996	0.995	0.999	0.996	0.991	0.994	0.998
	χ^2	0.353	0.0171	0.092	0.18	0.01	0.16	0.38	0.16	0.03
	E (kJ/mol)	7.93	5.52	4.84	9.44	8.90	7.76	10.78	10.31	9.12

16 kJ/mol that primarily reflect physical, essentially weakened chemical-based, or a combination between chemical and physical, and essentially powerful chemical-based processes, respectively.[56] The values detected of E for the CR retention by ZA fall within the limits of determined energy levels for physical mechanisms (<8 kJ/mol) and the span of zeolitic ion exchange mechanisms (0.6−25 kJ/mol), as supported by the theoretical findings from the kinetic examinations (Table 3).[53] The determined E parameter for CR retention behaviors through CH/Z and CD/Z aligns with the outlined energies for cooperative processes involving both chemical and physical interactions (8−16 kJ/mol) (Table 3).

2.2.3.4. Advanced Isotherm Modeling. The employing of statistical physics principles for equilibrium modeling of adsorption behaviors has the capacity to offer a deep understanding of the distinctive characteristics of adsorption reactions. These mathematical models assess the interactions involving soluble pollutants and the external groups throughout the interfaces of solid adsorption agents. The mathematical models implemented in this study include several computing functions that effectively illustrate the basic mechanisms, involving energetic and steric aspects. The steric factors that are established by the models are the numbers of CR that filled each receptor site (n), the total number of sites filled with CR across the ZA, CH/Z, and CD/Z interfaces (N_m), and the highest possible uptake efficiency of CR by ZA, CH/Z, and CD/Z after their fully saturated conditions (Q_{sat}). The energetic parameters include internal energy (E_{int}), entropy (S_a), uptake energy (E), and enthalpy (G). The assessment of such concepts, which were used to analyze the elimination activities of CR, encompassed the utilization of nonlinear regression analysis employing the illustrated equations developed for the respective models. The analysis mentioned above was adequately conducted by using multivariable nonlinear regression analysis in conjunction with the Levenberg−Marquardt iterative approach. The established degrees of fitness were afterward employed to evaluate and describe the adsorption behaviors of CR via ZA, CH/Z, and CD/Z using a monolayer model with a single energetic site. Table 4 as well as Figure 8 display the calculated parameters together with fitting variables.

2.2.3.4.1. Steric Properties

2.2.3.4.1.1. Number of Adsorbed CR ($n_{(CR)}$) per Each Site

The numerical results of the $n_{(CR)}$ parameter strongly reveal the orientation properties of the retained CR molecules across the outermost surfaces of ZA, CH/Z, and CD/Z (either vertically or horizontally), in addition to their significance with regard to the affecting mechanisms (either multidocking or multi-interactions). Activities that have the greatest impact through multianchorage or multidocking functions include the retention of a single CR ion through several retention sites. Retaining reactions that possess values smaller than 1 are correlated to the horizontal arrangement of these retained ions. On the other hand, the operations that exhibit values greater than 1 suggest the retention of CR in nonparallel forms and a vertical position. The uptake reactions in these systems are most significantly impacted by multimolecular mechanisms, where numerous dye ions have been captured by just one site.[64] The calculated values of n during the sequestration of CR by ZA ($n_{(CR)}$ = 2.31−3.17) are higher than 1 (Figure 9A−C; Table 4). The total number of retained CR molecules by one site across the outermost layers of CH/Z ($n_{(CR)}$ = 2.51−3.54) and CD/Z ($n_{(CR)}$ = 2.28−2.8) was similarly detected at

https://doi.org/10.1021/acsomega.4c01134
ACS Omega 2024, 9, 21204−21220

Table 4. Mathematical Parameters of the Addressed Advanced Isotherm Model (Monolayer Model of One Energy)

steric and energetic parameters				
		293 K	303 K	313 K
ZA	R^2	0.998	0.998	0.999
	RMSE	0.048	0.086	0.0137
	n	2.31	3.045	3.17
	I_m (mg/g)	60.67	34.66	29.43
	Q_{Sat} (mg/g)	140.3	110.04	89.6
	$C_{1/2}$ (mg/L)	58.8	69.57	75.38
	ΔE (kJ/mol)	−9.38	−13.9	−16.49
CH/Z	R^2	0.999	0.998	0.998
	RMSE	0.0413	0.0948	0.100
	n	2.51	2.89	3.54
	N_m (mg/g)	83.15	61.85	42.57
	Q_{Sat} (mg/g)	208.73	178.74	151.54
	$C_{1/2}$ (mg/L)	46.89	47.28	51.33
	ΔE (kJ/mol)	−13.06	−13.48	−13.71
CD/Z	R^2	0.996	0.993	0.995
	RMSE	0.151	0.203	0.122
	n	2.28	2.48	2.80
	N_m (mg/g)	98.08	77.96	58.75
	Q_{Sat} (mg/g)	223.6	193.36	164.50
	$C_{1/2}$ (mg/L)	42.16	42.80	46.31
	ΔE (kJ/mol)	−13.32	−13.73	−13.98

levels higher than 1 (Figure 9A−C; Table 4). Consequently, the CR dye was adsorbed by a multimolecular mechanistic pathway. Each retention site throughout ZA, CH/Z, and CD/Z had the capacity to accept several ions that were arranged in vertical arrangements with nonparallel features. Each receptor over the outermost layer of ZA and CH/Z has the capacity to accept a maximum of 4 CR ions, but every single receptor across the exterior of CD/Z is able to accept only 3 ions. This indicates substantial modifications in the surface characteristics of ZA during the hybridization process. The $n_{(CR)}$ estimations for ZA, CH/Z, and CD/Z in terms of the testing temperature effects reveal a remarkable increase with temperature from 293 to 313 K. The observed behavior was frequently ascribed to the assumed enhancement in the CR aggregating properties whenever it was adsorbed by ZA, CH/Z, and CD/Z at higher temperatures.[60] This also demonstrates the existence of thermal activation processes before the sequestration of CR using ZA, CH/Z, and CD/Z.[65,66]

2.2.3.4.1.2. Occupied Active Sites Density (N_m)

The densities of CR-consumed receptors ($N_{m\ (CR)}$) for ZA, CH/Z, and CD/Z are a valid indicator of the total number of unbound and effective adsorbing receptors over the surfaces of their particulates throughout the entire reaction (Figure 9D−F; Table 4). According to ZA's estimation, the $N_{m\ (CR)}$ quantities at different temperatures are 60.67 mg/g (293 K), 34.66 mg/g (303 K), and 29.43 mg/g (313 K) (Figure 9D; Table 4). The levels encountered a substantial rise following the combination of ZA with CH (CH/Z), attaining 83.15 mg/

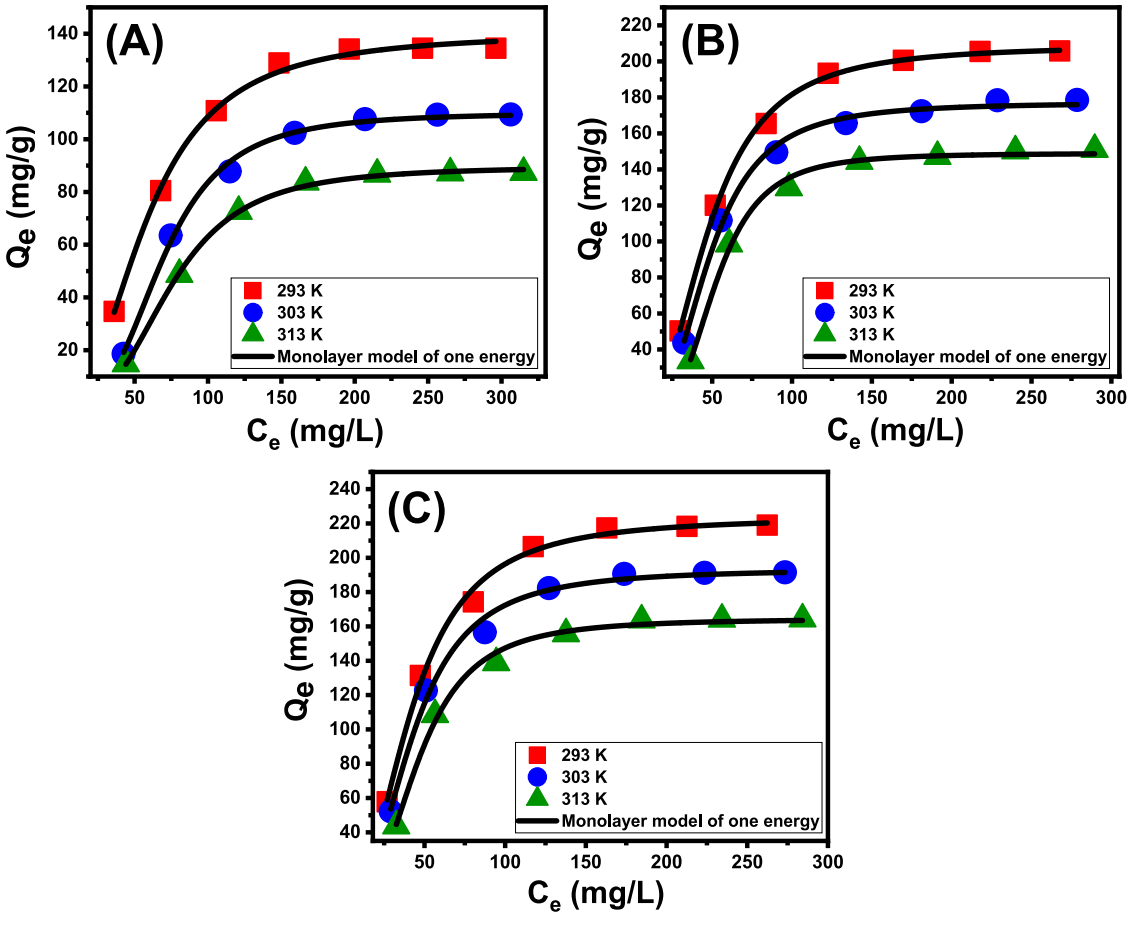

Figure 8. Fitting of the CR adsorption results with the advanced Monolayer model with one site of energy (ZA (A), CH/Z (B), and CD/Z (C)).

https://doi.org/10.1021/acsomega.4c01134
ACS Omega 2024, 9, 21204−21220

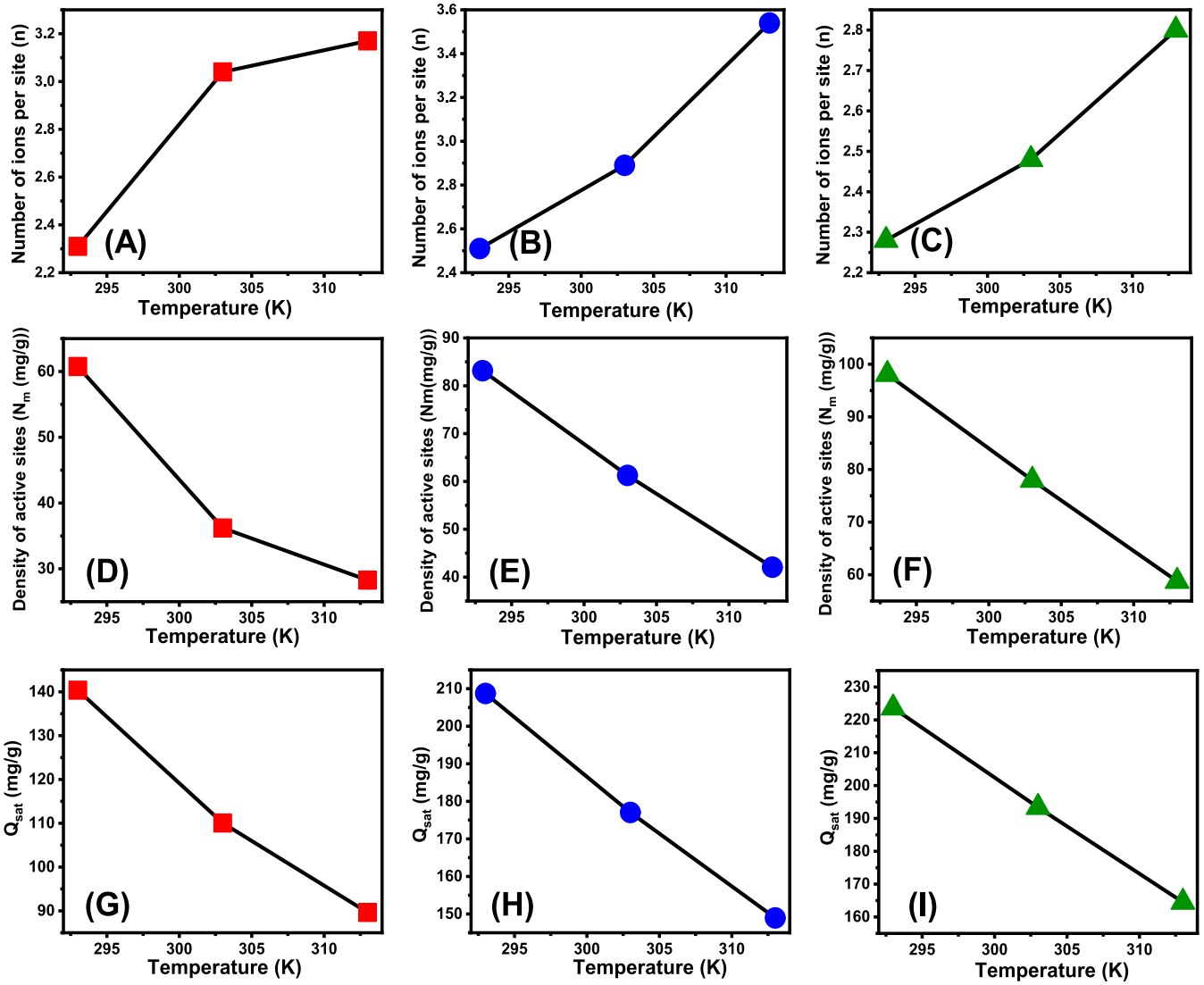

Figure 9. Change in the steric parameters during the uptake of CR involving the number of adsorbed CR molecules into single uptake site (ZA (A), CH/Z(B), and CD/Z (C)), occupied sites density (ZA (D), CH/Z (E), and CD/Z (F)), and saturation uptake capacities (ZA (G), CH/Z (H), and CD/Z (I)).

g at 293 K, 61.85 mg/g at 303 K, and 42.57 mg/g at 313 K (Figure 9E; Table 4). The increase in performance was also noticed after the incorporation of β-CD, with values of 98.1 mg/g (293 K), 77.9 mg/g (303 K), and 58.75 mg/g (313 K) (Figure 9F; Table 4). These findings strongly confirm an enormous rise in the number of present receptors following the binding of CH and β-CD. The boost in surface area, along with the insertion of actively functioning chemical groups into the blends, results in an enhanced reaction or contact interface involving the soluble dye ions and the blends' surfaces. The $N_{m\ (CR)}$ quantities for ZA, CH/Z, and CD/Z exhibit temperature-dependent reversibility in terms of their response to temperature (Figure 6E−H; Table 4). This matches the reported behaviors of $n_{(CR)}$, considering that the increase in the aggregating affinities leads to a reduction in the total quantity of filled receptors, alongside the influence of temperature on the prevailing activity of the reacting active receptors.[65,67]

2.2.3.4.1.3. Adsorption Capacity at the Saturation State of (Q_{sat})

The saturated adsorption characteristics of ZA, CH/Z, and CD/Z (Q_{sat}) reveal the expected value of the maximal sequestration capacity with the highest acceptability. Two key factors control the quantities of Q_{sat}: the established densities of the filled receptors (N_m) and the number of CR ions acquired by one receptor (n). ZA, being a possible adsorbent of CR, exhibits Q_{sat} levels of 140.3 mg/g at 293 K, 110.04 mg/g at 303 K, and 89.6 mg/g at 313 K (Figure 9G; Table 4). The use of CH/Z demonstrates expected saturated capacities of 208.7 mg/g (at 293 K), 178.7 mg/g (at 303 K), and 151.54 mg/g (at 313 K) (Figure 9H and Table 4). The use of CD/Z hybrids exhibited enhanced efficacy with values of 223.6 mg/g at 293 K, 193.36 mg/g at 303 K, and 164.5 mg/g at 313 K (Figure 9; Table 4). The exothermic characteristics of CR retention activities using ZA, CH/Z, and CD/Z are detected by the negative impact of temperature. This also suggests that as adsorbing temperature increases, the impact of thermal collisions becomes more pronounced, leading to a reduction in the efficiency of CR binding.[64] Moreover, the observed features of Q_{sat} that arise from the variation in temperature indicate a similarity to the designated behaviors of N_m rather than n. This suggests that the efficacy of CR

https://doi.org/10.1021/acsomega.4c01134
ACS Omega 2024, 9, 21204−21220

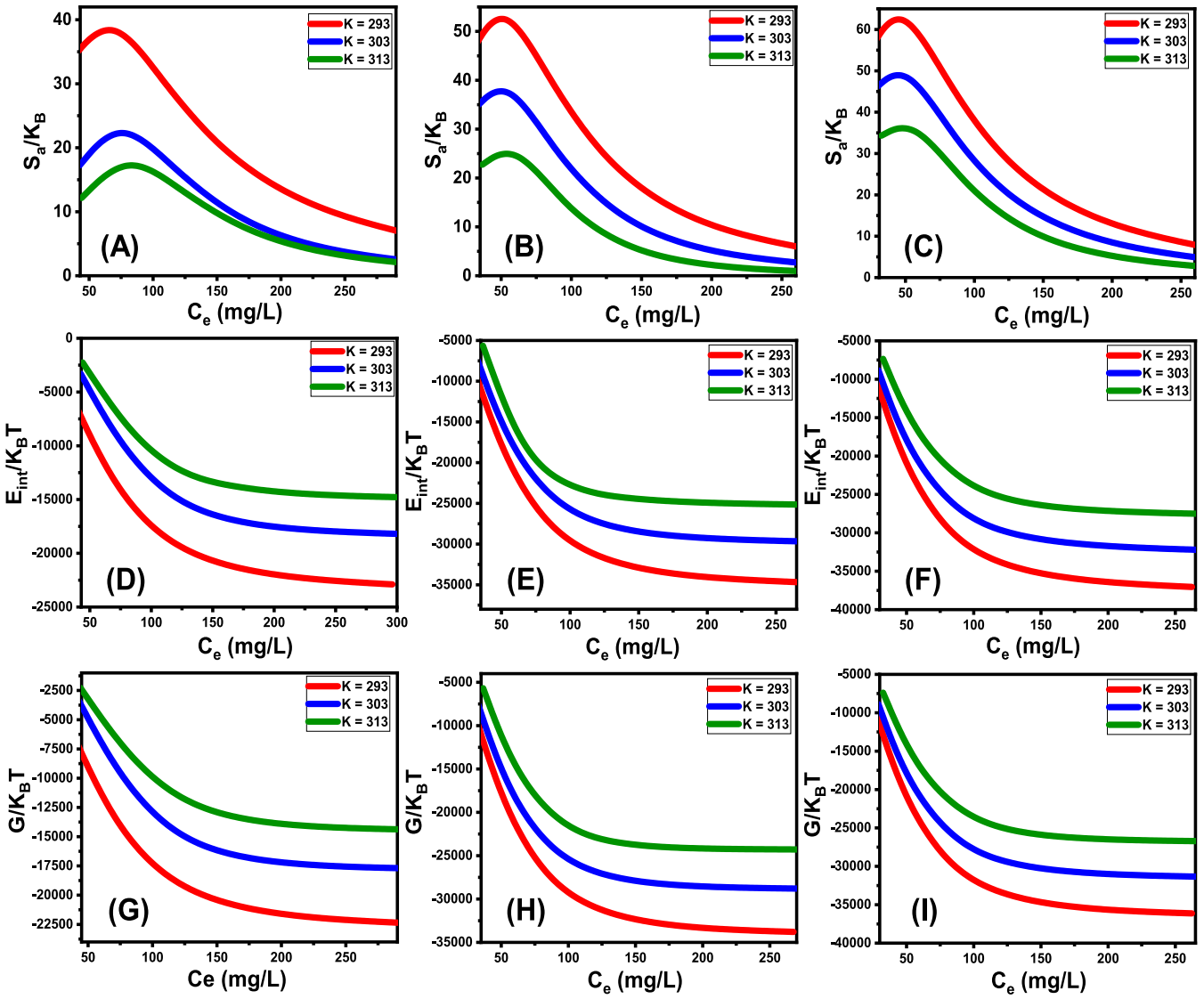

Figure 10. Change in the thermodynamic parameters during the uptake of CR involving entropy (ZA (A), CH/Z (B), and CD/Z (C)), internal energy (ZA (D), CH/Z (E), and CD/Z (F)), and free enthalpy (ZA (G), CH/Z (H), and CD/Z (I)).

retention is influenced by the active sites present rather than the potential of each individual active site.

2.2.3.4.2. Energetic Properties

2.2.3.4.2.1. Adsorption Energy

The energy changes (ΔE) associated with the uptake processes of CR can reliably indicate the underlying mechanisms; they correspond to either physical or chemical operations. The physical reactions possess energies below 40 kJ/mol, but the chemical pathways possess energies over 80 kJ/mol. The adsorption energy levels are employed to classify various types of physically existing mechanistic events. Such physical interactions described encompass coordination exchange (40 kJ/mol), hydrogen bonds (<30 kJ/mol), dipole binding interactions (2−29 kJ/mol), van der Waals interactions (4−10 kJ/mol), and hydrophobic binding (5 kJ/mol).[60,68] The CR eliminating energies (ΔE) had been theoretically determined utilizing eq 1, which incorporates the solubility metrics of CR within the water-based solution (S), gas constant (R = 0.008314 kJ/mol·K), CR levels during the half-saturation settings of ZA, CH/Z, and CD/Z, and absolute temperature (T).[69]

$$\Delta E = RT \ln\left(\frac{S}{C}\right) \quad (1)$$

The calculated energy metrics for CR retention by ZA and CH/Z fluctuate between −9.38 to −16.49 kJ/mol and −13 to −13.7 kJ/mol, respectively (Table 4). The assumed values of CD/Z ranged from −13.3 to −13.9 kJ/mol (Table 4). Therefore, the main mechanisms contributing to the adsorption of CR by ZA, CH/Z, and CD/Z comprised physical reactions, particularly dipole binding interactions (2 to 29 kJ/mol) and hydrogen bonds (<30 kJ/mol) for CH/Z and CS/Z. For ZA, the previous mechanism in addition to van der Waals forces (4 to 10 kJ/mol) significantly affects the uptake of CR dye. Furthermore, the reported negative signs of the assumed values of E throughout the sequestration of CR by ZA, CH/Z, and CD/Z align with the previously reported experimental data about the exothermic nature of these processes.

2.2.3.4.3. Thermodynamic Functions

2.2.3.4.3.1. Entropy

https://doi.org/10.1021/acsomega.4c01134
ACS Omega 2024, 9, 21204−21220

The entropy (S_a) corresponding to the CR retention processes by ZA, CH/Z, and CD/Z provides an obvious illustration of the order and disorder characteristics of the outermost surfaces of their nanostructures when subjected to different levels of dye ions, in addition to the specified reaction temperature. The S_a characteristics were illustrated by implementing the results obtained from eq 2, including the previously established measurements of N_m and n, in addition to the predicted contents of CR throughout the half-saturation states of ZA, CH/Z, and CD/Z ($C_{1/2}$).

$$\frac{S_a}{K_B} = N_m\left\{\ln\left(1 + \left(\frac{C}{C_{1/2}}\right)^n\right) - n\left(\frac{C}{C_{1/2}}\right)^n \frac{\ln\left(\frac{C}{C_{1/2}}\right)}{1 + \left(\frac{C}{C_{1/2}}\right)^n}\right\} \quad (2)$$

Based on the displayed curves, the entropy levels (S_a) decrease dramatically when CR is adsorbed into ZA, CH/Z, and CD/Z, particularly when the CR contents are very high (Figure 10A−C). This trend demonstrates a significant reduction in the disorder features of the interfaces of ZA, CH/Z, and CD/Z whenever the tracked CR levels increase. The entropy functions further support the effective docking of CR into the ZA, CH/Z, and CD/Z vacant and active interacting receptors, even if low quantities of dye molecules are present.[67,69] The highest levels of entropy have been detected during the capture of CR by ZA at equilibration concentrations of 67.8 mg/L (293 K), 74.6 mg/L (303 K), and 80.5 mg/L (313 K) (Figure 10A). The equilibration values for maximum entropy throughout the removal of CR through CH/Z are as follows: 51.9 mg/L at 293 K, 55.3 mg/L at 303 K, and 60.5 mg/L at 313 K (Figure 10B). The use of CD/Z reveals maximum entropy at CR levels of 47.4 mg/L (at 293 K), 50.9 mg/L (at 303 K), and 56.5 mg/L (at 313 K) (Figure 10C). These equilibrium values closely resemble the concentrations expected throughout the half-saturation phases of ZA, CH/Z, and CD/Z. Consequently, more CR ions lack the ability to dock at the still-available sites. Further, the significant reductions in the observed entropy levels indicated a substantial drop in the number of available sites along with a notable decline in the CR ions' mobility and diffusion properties.[70]

2.2.3.4.3.2. Internal Energy and Free Enthalpy

The study assessed the internal energy (E_{int}) correlated with the binding reactions of ZA, CH/Z, and CD/Z, alongside the qualities of free enthalpy (G) and the manner in which they are affected by changes in dye contents and operating temperature. The evaluation was conducted using values obtained from eqs 3 and 4, which were computed using the earlier established N_m, n, and $C_{1/2}$, along with the translation partition (Z_v).[66]

$$\frac{E_{int}}{K_B T} = nN_m\left[\left(\frac{\left(\frac{C}{C_{1/2}}\right)^n \ln\left(\frac{C}{Z_v}\right)}{1 + \left(\frac{C}{C_{1/2}}\right)^n}\right) - \left(\frac{n \ln\left(\frac{C}{C_{1/2}}\right)\left(\frac{C}{C_{1/2}}\right)^n}{1 + \left(\frac{C}{C_{1/2}}\right)^n}\right)\right] \quad (3)$$

$$\frac{G}{K_B T} = nN_m \frac{\ln\left(\frac{C}{Z_v}\right)}{1 + \left(\frac{C_{1/2}}{C}\right)^n} \quad (4)$$

The calculated values of E_{int} with respect to CR retention processes via ZA, CH/Z, and CD/Z possess negative signs, and these findings reveal a significant decrease whenever the temperature is increased from 293 to 303 K (Figure 10D−F). This validates the spontaneous alongside exothermic characteristics of the CR elimination processes via ZA, CH/Z, and CD/Z. Similar behaviors and properties have been identified for the described levels and behaviors of enthalpy. The G results have negative signs and demonstrate a reversible correlation with the practical retention temperature (Figure 10G−I). This suggests a decrease in the feasibility features and confirms the spontaneity and exothermic behaviors of the CR sequestration using ZA, CH/Z, and CD/Z.

2.2.4. Recyclability. The ability of CH/Z and CD/Z hybrids to be successfully used as adsorbents for CR has been examined, emphasizing their recyclability, which is a key consideration in evaluating their suitability for commercial and practical uses. The CH/Z and CD/Z nanostructures were extensively washed using distilled water for a duration of 10 min, and this procedure was repeated five times. The CH/Z and CD/Z were then subjected to drying at a temperature of 60 °C over a duration of 10 h in order to facilitate their potential utilization in additional CR decontamination rounds. The recyclability studies were conducted with specific parameters: pH 3, a mass of 0.40 g/L, a period of 24 h, a volume of 100 mL, CR concentrations of 350 mg/L, and a temperature of 293 K. The results of the five experimental rounds conducted to assess the recycling of CH/Z and CD/Z as adsorbents demonstrate consistent and remarkable efficacy in adsorbing CR, with remarkable stability and adequate recyclability properties (Figure 11). The CH/Z material

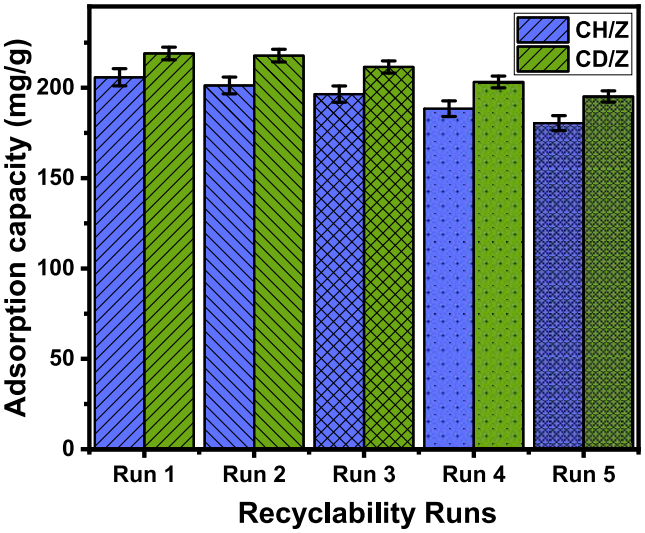

Figure 11. Recyclability properties of CH/Z and CD/Z composites during the elimination of CR dye.

demonstrated significant recyclable qualities that resulted in a removal efficiency of 205.8 mg/g (Cycle 1), 201.3 mg/g (Cycle 2), 196.5 mg/g (Cycle 3), 188.4 mg/g (Cycle 4), and 180.4 mg/g (Cycle 5). The decontamination process of CR yielded eliminating capacities of 219 mg/g (Cycle 1), 217.8 mg/g (Cycle 2), 211.5 mg/g (Cycle 3), 203.2 mg/g (Cycle 4), and 195.2 mg/g (Cycle 5) during the recycling of CD/Z.

https://doi.org/10.1021/acsomega.4c01134
ACS Omega 2024, 9, 21204−21220

3. CONCLUSIONS

Synthetic zeolite-A was successfully hybridized with two types of polymers, including chitosan and β-cyclodextrin. The influence of the two polymers on the adsorption performances of zeolite-A during the elimination of Congo red dye was evaluated in a synergetic manner. The hybridized products achieved higher performances (223.6 mg/g (CD/Z) and 208.7 mg/g (CH/Z)) than the single zeolite-A phase (140.3 mg/g). This enhancement impact was assigned to the enhancement in the organophilic properties of the zeolite surface in addition to the surface area and the quantities of existing adsorption receptors. This was supported by the findings of advanced isotherm modeling and related steric factors. While the zeolite particles exhibit an active site density of 60 mg/g, the integration of CH and CD induces values of 83 and 98 mg/g, respectively. The Gaussian energies as well as the adsorption energies validate the uptake of CR into CD/Z and CH/Z hybrids by physical mechanisms, mainly dipole bonding (2−29 kJ/mol) and hydrogen bonding (<30 kJ/mol). These mechanisms had exothermic and spontaneous properties.

4. EXPERIMENTAL WORK

4.1. Materials. The kaolinite powdered fractions that have been implemented in the zeolite synthesis process have been directly supplied through the Central Metallurgical and Development Institute in Egypt. The β-cyclodextrin (>85%), acetic acid (99.8%), ethanol (95%), and chitosan (MW 120,000; 85%) had been purchased through Sigma-Aldrich Egypt as high-purity items to be employed throughout the hybridization operations. Solutions of NaOH, HNO_3, and N_4OH with specified concentrations have been employed in the various fabrication and adjusting procedures without performing purification. The adsorption testing had been accomplished using Congo red synthetic dye (Sigma-Aldrich) as the primary source of synthetic dye contaminants.

4.2. Synthesis of Chitosan/Zeolite-A (CH/Z) and β-Cyclodextrin/Zeolite-A (CD/Z). The zeolite-A-synthesizing procedures were conducted following the methodology outlined by Shaban et al.[44] The kaolinite flour underwent thermal activation to produce metakaolinite (MK) through a 4-h heating step at a temperature of 750 °C. Subsequently, the MK output was subjected to dispersion throughout a NaOH solution over a duration of 12 h with continuous stirring at an approximate weight proportion of MK to NaOH equal to 1:2. The aluminosilicate gel obtained after this step was then transferred into a Teflon-lined stainless steel autoclave and subjected to hydrothermal processing at a temperature of 150 °C over a duration of 4 h. The synthesized product underwent filtration, followed by washing to neutralize the zeolite particulates, and was then dried at a temperature of 70 °C for 12 h.

The chitosan/zeolite-A hybrid (CH/Z) was produced following the methodologies described by Jiang et al.[36] A total of 4 g of zeolite particulates were evenly distributed throughout 100 mL of distilled water while exposed to 180 min of ultrasound treatments. It was then combined with the formerly produced chitosan colloid solution (CH (0.4 g) was dissolved in acetic acid (100 mL; 0.1 M)). The resulting slurry then underwent homogenization utilizing a highly successful mixing technique that involved 12 h of ultrasound treatment and magnetic stirring at 800 rpm. Subsequently, the product has undergone filtration, careful rinsing to mitigate the adverse consequences of any residual acetic acid, and gradual drying at a temperature of 60 °C for a duration of 12 h. The blend that had been produced was designated as CH/Z and was saved to perform the additional testing.

To produce the β-cyclodextrin/zeolite-A hybrid form, 4 g of developed zeolite was mixed well with distilled water using an ultrasound generator (240 W) alongside a magnetic stirrer for a duration of 60 min. In an equivalent test, 4 g of β-CD had to be dissolved in 100 mL of ethanol before being well mixed over 60 min. Following that, a 240 W ultrasonic generator was used to mix the β-CD solutions with the ZA slurry. The resulting mixture was then stirred for a duration of 24 h. After the blending time, the CD/Z particles were isolated from the remaining solutions using centrifugation at a speed of 3000 rpm over 15 min. Following a systematic rinse utilizing distilled water, the resulting material was then dried at a temperature of 60 °C for a duration of 12 h. Ultimately, the end result was designated as CD/Z and was employed in the subsequent experimental procedures.

4.3. Analytical Techniques. The crystallization levels along with crystal forms were determined using a PANalytical-Empyrean X-ray diffractometer, which detected patterns throughout the span of 0 to 70°. The chemical frameworks of ZA, CH/Z, and CD/Z have been identified utilizing a Fourier transform infrared spectrometer (FTIR8400S; Shimadzu) over a frequency range of 400 to 4000 cm^{-1}. Scanning electron microscopy (SEM) images were acquired promptly after applying thin gold films to ZA, CH/Z, and CD/Z, employing a Gemini Zeiss Ultra 55 microscope. These images were applied to follow the anticipated alterations in the morphological characteristics of ZA following the two distinct modifying procedures. Furthermore, the internal properties of ZA, CH/Z, and CD/Z were further examined using HRTEM images acquired by a transmission electron microscope (JEOL-JEM2100) at a voltage of acceleration of about 200 kV. The surface area and porosity of ZA, CH/Z, and CD/Z have been assessed by implementing a Beckman Coulter SA3100 surface area analyzer alongside the corresponding N_2 adsorption and desorption isotherms.

4.4. Adsorption Studies. The adsorption potential of ZA, CH/Z, and CD/Z as adsorbents for Congo red (CR) dye has been examined using several cycles of batch retention experiments. The study included many influencing factors, including pH levels ranging from 2 to 7, initial dye concentrations ranging from 50 to 400 mg/L, and retention durations ranging from 30 to 1440 min. The total volume of polluted solutions and the mass of Z, CH/Z, and CD/Z had been maintained constant at 100 mL and 0.4 g/L, respectively; however, the uptake temperature fluctuated between 293 and 313 K throughout the entire study. The adsorption data has been averaged based on the testing outcomes in triplicate, with standard deviations less than 2.9%. After the completion of all examinations, the remaining dye was analyzed employing a UV−vis spectrophotometer (V-760, JASCO International Co.; Japan) at a determination wavelength of 450 nm. The concentrations of dyes were measured to calculate the adsorbed capacities of CH/Z and CD/Z. This was done using eq 5, based on the treatment volume (V (L)), composites dose (m (g)), starting concentration (C_o (mg/L)), and residual concentration (C_e (mg/L)).

$$Q_{e(mg/g)} = \frac{(C_O - C_e)V}{m} \quad (5)$$

https://doi.org/10.1021/acsomega.4c01134
ACS Omega 2024, 9, 21204−21220

4.5. Theoretical Traditional and Advanced Equilibrium Studies. The adsorption behaviors have been simulated employing traditional kinetic, conventional isotherm, and modern isotherm (according to statistical physics assumptions) models (Table S1). The kinetic and conventional equilibrium modeling was performed employing nonlinear fitting approaches, applying the theoretical formulations of those models. The resulting outcomes for the coefficient of determination (R^2) (eq 6) and Chi-squared (χ^2) (eq 7) have been employed in the analysis. The appropriateness of the adsorption behaviors with the assessed advanced equilibrium models has been established via the coefficient of determination (R^2) alongside the root-mean-square error (RMSE) (eq 8). The letters m', p, $Q_{i,cal}$, and $Q_{i,exp}$ denote the experimental findings, studied parameters, anticipated CR uptake, and verified adsorption efficiency, respectively.

$$R^2 = 1 - \frac{\sum (Q_{e,exp} - Q_{e,cal})^2}{\sum (Q_{e,exp} - Q_{e,mean})^2} \quad (6)$$

$$\chi^2 = \sum \frac{(Q_{e,exp} - Q_{e,cal})^2}{Q_{e,cal}} \quad (7)$$

$$\mathrm{RMSE} = \sqrt{\frac{\sum_{i=1}^{m'} (Q_{e,cal} - Q_{e,exp})^2}{m' - p}} \quad (8)$$

■ ASSOCIATED CONTENT

Supporting Information

The Supporting Information is available free of charge at https://pubs.acs.org/doi/10.1021/acsomega.4c01134.

Nonlinear equations of kinetic, classic isotherm, and advanced isotherm mode (Table S1) (PDF)

■ AUTHOR INFORMATION

Corresponding Authors

Hassan Ahmed Rudayni − *Department of Biology, College of Science, Imam Mohammad Ibn Saud Islamic University (IMSIU), Riyadh 11623, Kingdom of Saudi Arabia*; Email: harudayni@imamu.edu.sa

Wail Al Zoubi − *Materials Electrochemistry Laboratory, School of Materials Science and Engineering, Yeungnam University, Gyeongsan 38541, Republic of Korea*; orcid.org/0000-0003-4213-8481; Email: wailalzoubi@ynu.ac.kr

Mostafa R. Abukhadra − *Materials Technologies and their Applications Lab, Geology Department, Faculty of Science, Beni-Suef University, Beni-Suef City 65211, Egypt; Geology Department, Faculty of Science, Beni-Suef University, Beni-Suef 65211, Egypt*; orcid.org/0000-0001-5404-7996; Phone: +2001288447189; Email: Abukhadra89@Science.bsu.edu.eg

Authors

Amna M. Farhan − *Materials Technologies and their Applications Lab, Geology Department, Faculty of Science, Beni-Suef University, Beni-Suef City 65211, Egypt; Chemistry Department, Faculty of Science, Beni-Suef University, Beni-Suef 65211, Egypt*

Gasem M. Abu-Taweel − *Department of Biology, College of Science, Jazan University, Jazan 45142, Saudi Arabia*

Islam R. Sayed − *Materials Technologies and their Applications Lab, Geology Department, Faculty of Science, Beni-Suef University, Beni-Suef City 65211, Egypt; Geology Department, Faculty of Science, Beni-Suef University, Beni-Suef 65211, Egypt*

Ahmed A. Allam − *Department of Biology, College of Science, Imam Mohammad Ibn Saud Islamic University (IMSIU), Riyadh 11623, Kingdom of Saudi Arabia*

Complete contact information is available at: https://pubs.acs.org/10.1021/acsomega.4c01134

Author Contributions

This article was written through the contributions of all authors. All authors have given their approval to the final version of the manuscript

Notes

The authors declare no competing financial interest.

■ ACKNOWLEDGMENTS

This work was supported and funded by the Deanship of Scientific Research at Imam Mohammad Ibn Saud Islamic University (IMSIU) (grant number IMSIU-RPP2023032).

■ REFERENCES

(1) Yang, J.; Chen, X.; Zhang, J.; Wang, Y.; Wen, H.; Xie, J. Role of chitosan-based hydrogels in pollutants adsorption and freshwater harvesting: A critical review. *Int. J. Biol. Macromol.* **2021**, *189*, 53−64.

(2) Zourou, A.; Ntziouni, A.; Adamopoulos, N.; Adamopoulos, N.; Roman, T.; Roman, T.; Zhang, F.; Zhang, F.; Terrones, M.; Terrones, M.; Kordatos, K. Graphene oxide-CuFe2O4 nanohybrid material as an adsorbent of Congo red dye. *Carbon Trends* **2022**, *7*, No. 100147.

(3) Arab, C.; El Kurdi, R.; Patra, D. Zinc curcumin oxide nanoparticles for enhanced adsorption of Congo red: kinetics and adsorption isotherms study. *Mater. Today Chem.* **2022**, *23*, No. 100701.

(4) Jawad, A. H.; Malek, N. N. A.; Khadiran, T.; ALOthman, Z. A.; Yaseen, Z. M. Mesoporous high-surface-area activated carbon from biomass waste via microwave-assisted-H3PO4 activation for methylene blue dye adsorption: An optimized process. *Diamond Relat. Mater.* **2022**, *128*, No. 109288.

(5) Hassan, H. M. A.; El-Aassar, M. R.; El-Hashemy, M. A.; Betiha, M. A.; Alzaid, M.; Alqhobisi, A. N.; Alzarea, L. A.; Alsohaimi, I. H. Sulfanilic acid-functionalized magnetic GO as a robust adsorbent for the efficient adsorption of methylene blue from aqueous solution. *J. Mol. Liq.* **2022**, *361*, No. 119603.

(6) Taher, T.; Putra, R.; Palapa, N. R.; Lesbani, A. Preparation of magnetitenanoparticle-decorated NiFe layered double hydroxide and its adsorption performance for congo red dye removal. *Chem. Phys. Lett.* **2021**, *777*, No. 138712, DOI: 10.1016/j.cplett.2021.138712.

(7) Shemy, M. H.; Othman, S. I.; Alfassam, H. E.; Al-Waili, M. A.; Alqhtani, H. A.; Allam, A. A.; Abukhadra, M. R. Synthesis of green magnetite/carbonized coffee composite from natural pyrite for effective decontamination of congo red dye: Steric, synergetic, oxidation, and ecotoxicity studies. *Catalysts* **2023**, *13* (2), 264.

(8) Pathania, D.; Dhar, S.; Sharma, A.; Srivastava, A. K. Decolourization of noxious safranin-T from waste water using Mangifera indica as precursor. *Environ. Sustainability* **2021**, *4*, 355−364.

(9) Indira, K.; Shanmugam, S.; Hari, A.; Vasantharaj, S.; Sathiyavimal, S.; Brindhadevi, K.; El Askary, A.; Elfasakhany, A.; Pugazhendhi, A. Photocatalytic degradation of congo red dye using nickel−titanium dioxide nanoflakes synthesized by Mukia madrasapatna leaf extract. *Environ. Res.* **2021**, *202*, No. 111647.

(10) Benisha, R.; Amalanathan, M.; Aravind, M.; Mary, M. S. M.; Ahmad, A.; Tabassum, S.; Al-Qahtani, W. H.; Ahmad, I. Catharanthus roseus leaf extract mediated Ag-MgO nanocatalyst for photocatalytic degradation of Congo red dye and their antibacterial activity. *J. Mol. Struct.* **2022**, *1262*, No. 133005.
(11) Adly, E. R.; Shaban, M. S.; El-Sherbeeny, A. M.; Al Zoubi, W.; Abukhadra, M. R. Enhanced Congo Red Adsorption and Photo-Fenton Oxidation over an Iron-Impeded Geopolymer from Ferruginous Kaolinite: Steric, Energetic, Oxidation, and Synergetic Studies. *ACS Omega* **2022**, *7*, 31218−31232.
(12) Durrani, W. Z.; Nasrullah, A.; Khan, A. S.; Fagieh, T. M.; Bakhsh, E. M.; Akhtar, K.; Khan, S. B.; Din, I. U.; Khan, M. A.; Bokhari, A. Adsorption efficiency of date palm based activated carbon-alginate membrane for methylene blue. *Chemosphere* **2022**, *302*, No. 134793.
(13) Harja, M.; Buema, G.; Bucur, D. Recent advances in removal of Congo Red dye by adsorption using an industrial waste. *Sci. Rep.* **2022**, *12*, No. 6087, DOI: 10.1038/s41598-022-10093-3.
(14) Narayan, M.; Sadasivam, R.; Packirisamy, G.; Pichiah, S. Electrospun polyacrylonitrile-Moringa Olifera based nanofibrous bio-sorbent for remediation of Congo red dye. *J. Environ. Manage.* **2022**, *317*, No. 115294.
(15) Oladoye, P. O.; Ajiboye, T. O.; Omotola, E. O.; Oyewola, O. J. Methylene blue dye: Toxicity and potential elimination technology from wastewater. *Results Eng.* **2022**, *16*, No. 100678.
(16) Le, T. M. H.; Nuisin, R.; Mongkolnavin, R.; Painmanakul, P.; Sairiam, S. Enhancing Dye Wastewater Treatment Efficiency In Ozonation Membrane Contactors by Chloro- and Fluoro-Organo-silanes' Functionality on Hydrophobic Pvdf Membrane Modification. *SSRN Electr. J.* **2022**, *288*, 120711 DOI: 10.2139/ssrn.4007273.
(17) Roy, N.; Chakraborty, S. ZnO as photocatalyst: An approach to wastewater treatment. *Mater. Today: Proc.* **2021**, *46*, 6399−6403.
(18) Ashrafi, G.; Nasrollahzadeh, M.; Jaleh, B.; Sajjadi, M.; Ghafuri, H. Biowaste- and nature-derived (nano) materials: Biosynthesis, stability, and environmental applications. *Adv. Colloid Interface Sci.* **2022**, *301*, No. 102599.
(19) Basaleh, A. A.; Al-Malack, M. H.; Saleh, T. A. Poly (acrylamide acrylic acid) grafted on steel slag as an efficient magnetic adsorbent for cationic and anionic dyes. *J. Environ. Chem. Eng.* **2021**, *9*, No. 105126.
(20) Alam, G.; Ihsanullah, I.; Naushad, M.; Sillanpää, M. Applications of artificial intelligence in water treatment for optimization and automation of adsorption processes: Recent advances and prospects. *Chem. Eng. J.* **2022**, *427*, No. 130011.
(21) Lahiri, S. K.; Zhang, C.; Sillanpää, M.; Liu, L. Nanoporous NiO@SiO2 photo-catalyst prepared by ion-exchange method for fast elimination of reactive dyes from wastewater. *Mater. Today Chem.* **2022**, *23*, No. 100677.
(22) Ghanbari, S.; Fatehizadeh, A.; Khiadani, M.; Taheri, E.; Iqbal, H. M. N. Treatment of synthetic dye containing textile raw wastewater effluent using UV/Chlorine/Br photolysis process followed by activated carbon adsorption. *Environ. Sci. Pollut. Res.* **2022**, *29*, 39400−39409.
(23) Pandey, D.; Daverey, A.; Dutta, K.; Yata, V. K.; Arunachalam, K. Valorization of waste pine needle biomass into biosorbents for the removal of methylene blue dye from water: Kinetics, equilibrium and thermodynamics study. *Environ. Technol. Innovation* **2022**, *25*, No. 102200.
(24) Kenawy, E.-R.; Tenhu, H.; Khattab, S. A.; Eldeeb, A. A.; Azaam, M. M. Highly efficient adsorbent material for removal of methylene blue dye based on functionalized polyacrylonitrile. *Eur. Polym. J.* **2022**, *169*, No. 111138.
(25) Abukhadra, M. R.; Saad, I.; Othman, S. I.; Katowah, D. F.; Ajarem, J. S.; Alqarni, S. A.; Allam, A. A.; Al Zoubi, W.; Gun Ko, Y. Characterization of Fe^0@Chitosan/Cellulose structure as effective green adsorbent for methyl Parathion, malachite Green, and levofloxacin Removal: Experimental and theoretical studies. *J. Mol. Liq.* **2022**, *368*, No. 120730.
(26) Wang, L.; Muhammad, H.; Laipan, M.; Fan, X.; Guo, J.; Li, Y. Enhanced removal of Cr (VI) and Mo (VI) from polluted water using L-cysteine doped polypyrrole/bentonite composite. *Appl. Clay. Sci.* **2022**, *217*, No. 106387.
(27) Zhang, L.; Wang, C.; Yang, R.; Zhou, G.; Yu, P.; Sun, L.; Hao, T.; Wang, J.; Liu, Y. Novel environment-friendly magnetic bentonite nanomaterials functionalized by carboxymethyl chitosan and 1-(2-pyridinylazo)-2-naphthaleno for adsorption of Sc (III). *Appl. Surf. Sci.* **2021**, *566*, No. 150644.
(28) Gao, Y.; Karatas, Y. D.; Nouali, H.; Salomon, J. P.; Lalevée, J.; Simon-Masseron, A. Zeolite/Polymer Composites Prepared by Photopolymerization: Effect of Compensation Cations on Opacity and Gas Adsorption Applications. *Chem. − Eur. J.* **2023**, *30* (11), No. e202302229.
(29) Guo, J.; Wang, L.; Tu, Y.; Muhammad, H.; Fan, X.; Cao, G.; Laipan, M. Polypyrrole modified bentonite nanocomposite and its application in high-efficiency removal of Cr (VI). *J. Environ. Chem. Eng.* **2021**, *9* (6), No. 106631.
(30) Sandomierski, M.; Zielińska, M.; Voelkel, A. Calcium zeolites as intelligent carriers in controlled release of bisphosphonates. *Int. J. Pharm.* **2020**, *578*, No. 119117.
(31) Abukhadra, M. R.; Mostafa, M.; Jumah, M. N. B.; Al Khalawi, N.; Alruhaimi, R. S.; Salama, Y. F.; Allam, A. A. Correction: Insight into the Adsorption Properties of Chitosan/Zeolite A Hybrid Structure for Effective Decontamination of Toxic Cd (II) and As (V) Ions from the Aqueous Environments. *J. Polym. Environ.* **2022**, *30*, 4500.
(32) Servatan, M.; Zarrintaj, P.; Mahmodi, G.; Kim, S. J.; Ganjali, M. R.; Saeb, M. R.; Mozafari, M. Zeolites in drug delivery: Progress, challenges and opportunities. *Drug Discovery Today* **2020**, *25*, 642−656.
(33) Marković, M.; Daković, A.; Rottinghaus, G. E.; Kragović, M.; Petković, A.; Krajišnik, D.; Milić, J.; Mercurio, M.; de Gennaro, B. Adsorption of the mycotoxin zearalenone by clinoptilolite and phillipsite zeolites treated with cetylpyridinium surfactant. *Colloids Surf., B* **2017**, *151*, 324−332.
(34) Bandura, L.; Białoszewska, M.; Malinowski, S.; Franus, W. Adsorptive performance of fly ash-derived zeolite modified by β-cyclodextrin for ibuprofen, bisphenol A and caffeine removal from aqueous solutions − equilibrium and kinetic study. *Appl. Surf. Sci.* **2021**, *562*, No. 150160.
(35) Lu, S.; Liu, Q.; Han, R.; Shi, J.; Guo, M.; Song, C.; Ji, N.; Lu, X.; Ma, D. Core-shell structured Y zeolite/hydrophobic organic polymer with improved toluene adsorption capacity under dry and wet conditions. *Chem. Eng. J.* **2021**, *409*, No. 128194.
(36) Jiang, Y.; Abukhadra, M. R.; Refay, N. M.; Sharaf, M. F.; El-Meligy, M. A.; Awwad, E. M. Synthesis of chitosan/MCM-48 and β-cyclodextrin/MCM-48 composites as bio-adsorbents for environmental removal of Cd2+ ions.; kinetic and equilibrium studies. *React. Funct. Polym.* **2020**, *154*, No. 104675.
(37) Ibrahim, S. M.; Bin Jumah, M. N.; Othman, S. I.; Alruhaimi, R. S.; Al-Khalawi, N.; Yasser, F. S.; Allam, A. A.; Abukhadra, R. M. Synthesis of Chitosan/Diatomite Composite as an Advanced Delivery System for Ibuprofen Drug; Equilibrium Studies and the Release Profile. *ACS Omega* **2021**, *6* (20), 13406−13416, DOI: 10.1021/acsomega.1c01514.
(38) Saad, A. M.; Abukhadra, M. R.; Ahmed, S. A. K.; Elzanaty, A. M.; Mady, A. H.; Betiha, M. A.; Shim, J. J.; Rabie, A. M. Photocatalytic degradation of malachite green dye using chitosan supported ZnO and Ce−ZnO nano-flowers under visible light. *J. Environ. Manage.* **2020**, *258*, No. 110043.
(39) El-Zeiny, H. M.; Abukhadra, M. R.; Sayed, O. M.; Osman, A. H.; Ahmed, S. A. Insight into novel β-cyclodextrin-grafted-poly (N-vinylcaprolactam) nanogel structures as advanced carriers for 5-fluorouracil: Equilibrium behavior and pharmacokinetic modeling. *Colloids Surf., A* **2020**, *586*, No. 124197.
(40) Sadjadi, S.; Koohestani, F. Composite of β-cyclodextrin and bentonite clay: A promising support for Pd immobilization and

developing a catalyst for hydrogenation of nitroarenes under mild reaction condition. *J. Phys. Chem. Solids* **2021**, *151*, No. 109894.
(41) Krawczyk, K.; Silvestri, D.; Nguyen, N. H.; Ševců, A.; Łukowiec, D.; Padil, V. V.; Řezanka, M.; Černík, M.; Dionysiou, D. D.; Wacławek, S. Enhanced degradation of sulfamethoxazole by a modified nano zero-valent iron with a β-cyclodextrin polymer: Mechanism and toxicity evaluation. *Sci. Total Environ.* **2022**, *817*, No. 152888.
(42) El-Sherbeeny, A. M.; Ibrahim, S. M.; AlHammadi, A. A.; Soliman, A. T. A.; Shim, J. J.; Abukhadra, M. R. Effective retention of radioactive Cs^{+} and Ba^{2+} ions using β-cyclodextrin functionalized diatomite (β-CD/D) as environmental adsorbent; characterization, application, and safety. *Surf. Interfaces* **2021**, *26*, No. 101434.
(43) Jumah, M. N. B.; Eid, M. H.; AL-Huqail, A. A.; Mohammad, M. A.; Bin-Murdhi, N. S.; Abu-Taweel, G. M.; Altoom, N.; Allam, A. A.; AbuKhadra, M. R. Enhanced remediation of As (V) and Hg (II) ions from aqueous environments using β-cyclodextrin/MCM-48 composite: Batch and column studies. *J. Water Process. Eng.* **2021**, *42*, No. 102118.
(44) Shaban, M.; Abukhadra, M. R.; Shahien, M. G.; Khan, A. A. P. Upgraded modified forms of bituminous coal for the removal of safranin-T dye from aqueous solution. *Environ. Sci. Pollut. Res.* **2017**, *24* (22), 18135−18151.
(45) Treacy, M. M.; Higgins, J. B. *Collection of Simulated XRD Powder Patterns for Zeolites*, 5th ed.; Elsevier, 2007.
(46) Altoom, N.; Ibrahim, S. M.; Othman, S. I.; Allam, A. A.; Alqhtani, H. A.; Al-Otaibi, F. S.; Abukhadra, M. R. Characterization of β-cyclodextrin/phillipsite (β-CD/Ph) composite as a potential carrier for oxaliplatin as therapy for colorectal cancer; loading, release, and cytotoxicity. *Colloids Surf., A* **2022**, *648*, No. 129144.
(47) Belviso, C.; Orlando, S.; Lettino, A.; Cavalcante, F.; Guarnaccio, A. Zeolite A with waste material: Morphological effect of laser treatments in air. *Process Saf. Environ. Prot.* **2024**, *182*, 845−856.
(48) Vivas, E. L.; Cho, K. Efficient adsorptive removal of Cobalt (II) ions from water by dicalcium phosphate dihydrate. *J. Environ. Manage.* **2021**, *283*, No. 111990.
(49) Tran, T. N.; Do, Q. C.; Kim, D.; Kim, J.; Kang, S. Urchin-like structured magnetic hydroxyapatite for the selective separation of cerium ions from aqueous solutions. *J. Hazard. Mater.* **2022**, *430*, No. 128488.
(50) Chen, Y.; Nie, Z.; Gao, J.; Wang, J.; Cai, M. A novel adsorbent of bentonite modified chitosan-microcrystalline cellulose aerogel prepared by bidirectional regeneration strategy for Pb (II) removal. *J. Environ. Chem. Eng.* **2021**, *9* (4), No. 105755.
(51) Abdel Salam, M.; Mokhtar, M.; Albukhari, S. M.; Baamer, D. F.; Palmisano, L.; Jaremko, M.; Abukhadra, M. R. Synthesis and Characterization of Green ZnO@ polynaniline/Bentonite Tripartite Structure (G. Zn@ PN/BE) as Adsorbent for As (V) Ions: Integration, Steric, and Energetic Properties. *Polymers* **2022**, *14* (12), 2329.
(52) El Qada, E. Kinetic Behavior of the Adsorption of Malachite Green Using Jordanian Diatomite as Adsorbent. *Jordanian J. Eng. Chem. Ind. (JJECI)* **2020**, *3* (1), 1−10, DOI: 10.48103/jjeci3120220.
(53) Salam, M. A.; Abukhadra, M. R.; Mostafa, M. Effective decontamination of As (V), Hg (II), and U (VI) toxic ions from water using novel muscovite/zeolite aluminosilicate composite: adsorption behavior and mechanism. *Environ. Sci. Pollut. Res.* **2020**, *27* (12), 13247−13260.
(54) Lin, X.; Xie, Y.; Lu, H.; Xin, Y.; Altaf, R.; Zhu, S.; Liu, D. Facile preparation of dual La-Zr modified magnetite adsorbents for efficient and selective phosphorus recovery. *Chem. Eng. J.* **2021**, *413*, No. 127530.
(55) Albukhari, S. M.; Salam, M. A.; Abukhadra, M. R. Effective retention of inorganic Selenium ions (Se (VI) and Se (IV)) using novel sodalite structures from muscovite.; characterization and mechanism. *J. Taiwan Inst. Chem. Eng.* **2021**, *120*, 116−126.
(56) Sayed, I. R.; Farhan, A. M.; AlHammadi, A. A.; El-Sayed, M. I.; Abd El-Gaied, I. M.; El-Sherbeeny, A. M.; Al Zoubi, W.; Ko, Y. G.; Abukhadra, M. R. Synthesis of novel nanoporous zinc phosphate/hydroxyapatite nano-rods (ZPh/HPANRs) core/shell for enhanced adsorption of Ni2+ and Co2+ ions: Characterization and application. *J. Mol. Liq.* **2022**, *360*, No. 119527.
(57) Sherlala, A.; Raman, A.; Bello, M. M.; Buthiyappan, A. Adsorption of arsenic using chitosan magnetic graphene oxide nanocomposite. *J. Environ. Manage.* **2019**, *246*, 547−556.
(58) Huang, Y.; Zeng, X.; Guo, L.; Lan, J.; Zhang, L.; Cao, D. Heavy metal ion removal of wastewater by zeolite-imidazolate frameworks. *Sep. Purif. Technol.* **2018**, *194*, 462−469.
(59) Jasper, E. E.; Ajibola, V. O.; Onwuka, J. C. Nonlinear regression analysis of the sorption of crystal violet and methylene blue from aqueous solutions onto an agro-waste derived activated carbon. *Appl. Water Sci.* **2020**, *10* (6), No. 132.
(60) Ashraf, M.-T.; AlHammadi, A. A.; El-Sherbeeny, A. M.; Alhammadi, S.; Al Zoubi, W.; Ko, Y. G.; Abukhadra, M. R. Synthesis of cellulose fibers/Zeolite-A nanocomposite as an environmental adsorbent for organic and inorganic selenium ions.; Characterization and advanced equilibrium studies. *J. Mol. Liq.* **2022**, *360*, No. 119573.
(61) Abukhadra, M. R.; Dardir, F. M.; Shaban, M.; Ahmed, E. A.; Soliman, M. F. Superior removal of Co2+, Cu2+ and Zn2+ contaminants from water utilizing spongy Ni/Fe carbonate−fluorapatite.; preparation, application and mechanism. *Ecotoxicol. Environ. Saf.* **2018**, *157*, 358−368.
(62) Shaban, M.; Sayed, M. I.; Shahien, M. G.; Abukhadra, M. R.; Ahmed, Z. M. Adsorption behavior of inorganic-and organic-modified kaolinite for Congo red dye from water, kinetic modeling, and equilibrium studies. *J. Sol-Gel Sci. Technol.* **2018**, *87* (2), 427−441.
(63) Dawodu, G.; Akpomie, M. A. Equilibrium Isotherm Studies on the Batch Sorption of Copper (II) ions from Aqueous Solution unto Nsu Clay. *Int. J. Sci. Eng. Res.* **2012**, *3* (12), 1−7.
(64) Mobarak, M.; Ali, R. A.; Seliem, M. K. Chitosan/activated coal composite as an effective adsorbent for Mn (VII): Modeling and interpretation of physicochemical parameters. *Int. J. Biol. Macromol.* **2021**, *186*, 750−758.
(65) Yang, X.; Wang, J.; El-Sherbeeny, A. M.; AlHammadi, A. A.; Park, W.-H.; Abukhadra, M. R. Insight into the adsorption and oxidation activity of a ZnO/piezoelectric quartz core-shell for enhanced decontamination of ibuprofen: steric, energetic, and oxidation studies. *Chem. Eng. J.* **2022**, *431*, No. 134312.
(66) Dhaouadi, F.; Sellaoui, L.; Reynel-Ávila, H. E.; Landín-Sandoval, V.; Mendoza-Castillo, D. I.; Jaime-Leal, J. E.; Lima, E. C.; Bonilla-Petriciolet, A.; Lamine, A. B. Adsorption mechanism of Zn2+, Ni2+, Cd2+, and Cu2+ ions by carbon-based adsorbents: interpretation of the adsorption isotherms via physical modelling. *Environ. Sci. Pollut. Res.* **2021**, *28* (24), 30943−30954.
(67) Sellaoui, L.; Ali, J.; Badawi, M.; Bonilla-Petriciolet, A.; Chen, Z. Understanding the adsorption mechanism of Ag+ and Hg2+ on functionalized layered double hydroxide via statistical physics modeling. *Appl. Clay Sci.* **2020**, *198*, No. 105828.
(68) Ali, R. A.; Mobarak, M.; Badawy, A. M.; Lima, E. C.; Seliem, M. K.; Ramadan, H. New insights into the surface oxidation role in enhancing Congo red dye uptake by Egyptian ilmenite ore: Experiments and physicochemical interpretations. *Surf. Interfaces* **2021**, *26*, No. 101316.
(69) Dhaouadi, F.; Sellaoui, L.; Badawi, M.; Reynel-Ávila, H. E.; Mendoza-Castillo, D. I.; Jaime-Leal, J. E.; Bonilla-Petriciolet, A.; Lamine, A. B. Statistical physics interpretation of the adsorption mechanism of Pb2+, Cd2+ and Ni2+ on chicken feathers. *J. Mol. Liq.* **2020**, *319*, No. 114168.
(70) Sellaoui, L.; Guedidi, H.; SarraWjihi, S.; Reinert, L.; Knani, S.; Duclaux, L.; Lamine, A. B. Experimental and theoretical studies of adsorption of ibuprofen on raw and two chemically modified activated carbons: new physicochemical interpretations. *RSC. Adv.* **2016**, *6* (15), 12363−12373.

https://doi.org/10.1021/acsomega.4c01134
ACS Omega 2024, 9, 21204−21220